Computer Simulation of the Linear and Nonlinear Optical Susceptibilities of *p*-Nitroaniline in Cyclohexane, 1,4-Dioxane, and Tetrahydrofuran in Quadrupolar Approximation. II. Local Field Effects and Optical Susceptibilitities

H. Reis,* M. G. Papadopoulos, and A. Grzybowski†

Institute of Organic and Pharmaceutical Chemistry, National Hellenic Research Foundation, Vasileos Constantinou 48, GR-11635 Athens, Greece

Received: June 7, 2006; In Final Form: July 13, 2006

This is the second part of a study to elucidate the local field effects on the nonlinear optical properties of *p*-nitroaniline (pNA) in three solvents of different multipolar character, that is, cyclohexane (CH), 1,4-dioxane (DI), and tetrahydrofuran (THF), employing a discrete description of the solutions. By the use of liquid structure information from molecular dynamics simulations and molecular properties computed by high-level ab initio methods, the local field and local field gradients on *p*-nitroaniline and the solvent molecules are computed in quadrupolar approximation. To validate the simulations and the induction model, static and dynamic (non)-linear properties of the pure solvents are also computed. With the exception of the static dielectric constant of pure THF, a good agreement between computed and experimental refractive indices, dielectric constants, and third harmonic generation signals is obtained for the solvents. For the solutions, it is found that multipole moments up to two orders higher than quadrupole have a negligible influence on the local fields on pNA, if a simple distribution model is employed for the electric properties of pNA. Quadrupole effects are found to be nonnegligible in all three solvents but are especially pronounced in the 1,4-dioxane solvent, in which the local fields are similar to those in THF, although the dielectric constant of DI is 2.2 and that of the simulated THF is 5.4. The electric-field-induced second harmonic generation (EFISH) signal and the hyper-Rayleigh scattering signal of pNA in the solutions computed with the local field are in good to fair agreement with available experimental results. This confirms the effect of the "dioxane anomaly" also on nonlinear optical properties. Predictions based on an ellipsoidal Onsager model as applied by experimentalists are in very good agreement with the discrete model predictions. This is in contrast to a recent discrete reaction field calculation of pNA in 1,4-dioxane, which found that the predicted first hyperpolarizability of pNA deviated strongly from the predictions obtained using Onsager−Lorentz local field factors.

1. Introduction

The search for materials with large nonlinear optical properties is currently a very active area of research. Prospective molecular candidates are often characterized by measurements on liquid solutions by techniques such as electric-field-induced second harmonic generation (EFISH) or hyper-Rayleigh scattering. To extract the unperturbed molecular properties from the experimental results, a quantitative understanding of solvent effects is required. Especially for highly dipolar solutes, one of the most important effects is the local field effect, which may change effective molecular hyperpolarizabilities by factors of 2 or more in different solvents. There are two contributions to this effect: the first one is due to the fields created by the surrounding molecules, and is present in the absence of any external fields and may be termed permanent local field, and the second is associated with the attenuation of the external fields at the molecular sites due to the superposition with additionally induced fields in the surrounding molecules. To account for the latter effect, continuum models such as the Onsager model are often employed, which treats the solute as a polarizable dipole embedded in a continuum, described by the relative permittivity ϵ and the refractive index n of the solvent. This model will therefore only work well if dipole−dipole interactions dominate the solute−solvent interactions. One popular solvent, for which this is not the case, is 1,4-dioxane: although its relative permittivity is that of a nonpolar solvent, which reflects the vanishing dipole moment of the molecules in the energetically most stable conformation, it generally behaves like a slightly polar one. This behavior manifests itself, for example, in solvent-induced absorption or fluorescence band shifts (see, e.g., refs 1 and 2), electrooptical absorption and emission measurements,[3,4] and other phenomena that depend on the polarity of the solvent[5,6] and has been accounted for in the dipolar Onsager reaction field model by assigning a "microscopic" or "effective" permittivity of 6−7 to this solvent.[7,8] It was suggested that large higher multipoles of the solvent molecules[9] or the accumulation of polar conformers of 1,4-dioxane around the solute may be responsible for this behavior.[10] For example, large quadrupole moments of 1,4-dioxane have been invoked to explain the biexponential excited-state population decay of (1-(9-anthryl)-3-(4-dimethyl-aniline) propane) (ADMA) in this solvent. The biexponential decay of the excited-state population of ADMA is typical for polar solvents, while in nonpolar solvents it is monoexponential.[6]

There have also been theoretical studies of the local field in 1,4-dioxane. For example, Geerlings et al.[5] have used molecular simulation methods with nonpolarizable potentials to demonstrate that the reaction field on a polar 1,3-dioxane molecule

* To whom correspondence should be addressed. E-mail: hreis@eie.gr.
† Present address: Institute of Physics, Silesian University, ul. Uniwersytecka 4, 40-007 Katowice, Poland.

10.1021/jp063529c CCC: $33.50
Published on Web 08/24/2006

embedded in 1,4-dioxane solvent is similar to that obtained from Onsager's reaction field computed with an effective dielectric constant of 7. In contrast to these *linear* effects, reports on the dioxane anomaly on *nonlinear* effects are scarce. In a recent report of a computation of the first hyperpolarizability β of pNA in 1,4-dioxane solution in the framework of the discrete reaction field model, in which higher multipoles of the solvent are taken into account at least approximately by way of partial charges on the atoms, it was found that β of pNA in 1,4-dioxane is only about 30% larger than the computed property of the isolated molecule, which is more typical for a nonpolar solvent than an "effectively" polar solvent.

To clarify the effect of the multipolar fields of the solvent molecules on the hyperpolarizabilities of pNA at the molecular level, one should start from a realistic molecular model of the solution, for example, structures obtained from computer simulation methods, employing reliable potential parameters. By simulating the pure solvents and comparison of simulated quantities with experimental results, the quality of the simulation parameters can be checked. When simulated solution structures are used, the permanent local field can be calculated starting from the multipole moments and polarizabilities of the unperturbed molecules. Comparison of several solvents with different multipolar properties allows a deeper analysis and an assessment of the reliability of the obtained results. In this work, we sought to implement this program by simulating three different solvents, nonpolar cyclohexane, presumably quadrupolar 1,4-dioxane, and dipolar tetrahydrofuran, which has a similar relative permittivity as the "effective" permittivity sometimes employed for 1,4-dioxane in the Onsager model and whose molecular structure is similar to 1,4-dioxane. In the first part of the series,[11] we reported on the accurate computation of the gas-phase properties of the corresponding molecules, taking all the relevant effects into account. It was found that experimental properties of pNA, including the results of gas-phase EFISH measurements by Kaatz et al.,[12] could be reproduced with sufficient accuracy.

In this second part of the study, we simulated solutions of pNA in these solvents as well as the pure solvents. Similar work on pure liquids has been published previously[13−15] but was limited to the dipolar approximation. To explore the effects of quadrupole moments with the corresponding polarizabilities, we have extended this work to higher multipolar order, similarly to the computation of the local field in crystalline ice I_h reported by Batista et al.[16−18] In the next section, the methods applied for the simulations, the induction model, and the quantum mechanical calculations are described, in section 3, the results for the pure solvents and the solutions are presented, which is followed by a summary of the results of both parts of this study.

The solvents will be abbreviated by DI for 1,4-dioxane, THF for tetrahydrofuran, and CH for cyclohexane. The same abbreviations will be used to denote the molecules. In those cases where a distinction is deemed to be necessary, qualifiers such as "liquid" or "molecule" will be added.

2. Methods

For the computation of the nonlinear optical properties of molecules in liquid solutions, we employed the following three-step approach. First, representative liquid structures are generated by classical molecular simulation methods. In the second step, electric properties (multipole moments and polarizabilities), computed by ab initio methods, are assigned to the molecules and average local fields acting on the molecules in the simulated liquid structures are computed. Finally, the (hyper)polarizabilities are recomputed for the molecules subject to the average local fields. These effective properties then either can be used to compute the macroscopic susceptibilities of the liquids which can be directly compared to equivalent experimental susceptibilities or may be compared with experimental properties obtained from measured susceptibilities by application of some continuum local-field approach, as, for example, the Onsager model. The first procedure could be used for all the linear susceptibilities of the pure solvents as well as the third-harmonic generation (THG) signal of the solvents and solutions, while the second approach has been employed for the EFISH signal of pNA solutions.

TABLE 1: Simulated Systems: Edge Lengths L/Å of Cubic Simulation Box, Number of Molecules N_i in the Box, Corresponding Density ρ/(g mL^{-1}), and Approximate Simulation Time, τ/ns

liquid	N_i	L	ρ	t
pure CH	108	26.91	0.77389[a]	0.1
pure DI	216	31.32	1.02687[b]	0.1
pure DI	54	19.73	1.02687[b]	0.1
pure THF	150	27.37	0.881[c]	1.0
pNA in CH	1+149	27.77	0.77389	0.5
pNA in DI	1+149	30.08	1.02687	1.0
pNA in THF	1+149	27.37	0.881	1.0

[a] Reference 10. [b] Reference 53. [c] Reference 102.

2.1. Molecular Dynamics Simulation. To obtain the liquid structures, trajectories were calculated by classical molecular dynamics simulations with the DLPOLY program package,[19] using a Nosé Hoover thermostat[20] with a bath relaxation time constant of 0.5 ps and $T = 298$ K, to simulate a canonical (NVT) ensemble. Six different systems were considered: pure 1,4-dioxane (DI), pure cyclohexane (CH), pure tetrahydrofuran (THF), and solutions of pNA in each of these solvents; details of the boxes and simulation times are given in Table 1. The box sizes were chosen to correspond to the experimental densities of the pure liquids at 298 K and 1 atm. The mass fraction of pNA in the solutions is 0.0109, 0.0104, and 0.0127 for CH, DI, and THF solution, respectively. The effect of the solute on the density of the pure solvent is small and has been neglected. For DI, two boxes of different sizes were used to explore box size effects on the properties.

The all-atom force field developed by Jorgensen et al. (OPLS-AA)[21−22] has been applied for the simulations. This force field was specifically optimized for simulations of liquids and solutions and should therefore be applicable for our purpose. The standard expression for the potential energy U for this force field is[23,24]

$$U = U_b + U_a + U_t + U_{nb,C} + U_{nb,LJ} \quad (1)$$

where U_b and U_a are sums of harmonic terms describing intramolecular bond stretching and angle bending, U_t is a sum of the triple cosine series for dihedral angle distortions, both proper and improper, $U_{nb,C}$ describes the nonbonded Coulomb interactions due to unpolarizable partial charges, and $U_{nb,LJ}$ describes nonbonded short-range interactions by a Lennard-Jones 12-6 potential. All force field parameters were taken from the literature, except for the partial charges and two torsional parameters connected with the amino and the nitro group of pNA. The parameters and details of the method employed to determine the additional parameters of pNA are given in the Appendix. With the partial charges thus obtained, the dipole moment of pNA of the optimized gas-phase structure is close to the dipole moments of the optimized structures obtained in ref 11 with different self-consistent reaction field models but computed *without* the effect of solvation. The use of these

charges is a compromise between the effect of solvation, which would increase the partial charges, and the decreasing effect of torsion and wagging motions of the amino and nitro groups. This is a departure from the generally applied procedure for nonpolarizable force fields (NPFFs) to choose partial charges which yield 10−15% higher dipole moments of the minimum structure to account for the solvation effect but may be necessary for pNA because NPFFs are not able to model the decreasing effect of amino/nitro torsion and wagging on the dipole moment of this push−pull molecule correctly.

Periodic boundary conditions were employed for the nonbonded interactions, using the Ewald summation procedure, under conducting boundary conditions, for the long-range Coulomb interactions. The simulation time step was 1 fs, and the trajectories were stored in 0.2 ps intervals. Each system was equilibrated for 50 ps prior to recording, employing velocity scaling each 50 fs to speed up the equilibration process.

2.2. Induction Model for the Local Fields and Field Gradients. In the discrete local field approximation adopted here, a molecule in a liquid experiences local fields due to the charge distribution of the surrounding molecules. We assume that the overlap of electronic wave functions of different molecules can be neglected and the fields of the molecular charge distribution can be approximated by a multipole expansion, taking into account at least the second moment or quadrupole moment, which is the first nonvanishing moment for nondipolar molecules such as DI and CH. We have used the traced definition of the multipole moments in our calculations[25−28]

$$M^{(n)}_{i_1,\ldots i_n} = \frac{1}{n!}\int \rho(\underline{r}) r_{i_1}\ldots r_{i_n}\, \mathrm{d}^3 r \tag{2}$$

where $\rho(r)$ is the molecular charge distribution and $M^{(n)}_{i_1,\ldots,i_n}$ is an element of the multipole moment in Cartesian coordinates, with $M^{(1)} \equiv \mu$ the dipole, $M^{(2)} \equiv Q$ the quadrupole, $M^{(3)} \equiv O$ the octopole, and $M^{(3)} \equiv H$ the hexadecapole moment. The advantages of using traced instead of traceless multipoles, as introduced by Buckingham,[29] have been pointed out, for example, by Logan[27] and Gunning and Raab.[28] All multipole moments refer to the center of nuclear charge.

For consistency reasons, field gradient effects should be considered, too, if the contribution of the second moment to the field is taken into account. The effective dipole, $\underline{\mu}^{\mathrm{eff}}_k$, and quadrupole moments, $\underline{\underline{Q}}^{\mathrm{eff}}_k$, of a molecule at site k in the liquid are approximated in terms of the corresponding free molecule properties by

$$\mu^{\mathrm{eff}}_{k,i} = \mu^{(0)}_{k,i} + \alpha^{(11)}_{k,ij} F_{k,j} + \alpha^{(12)}_{k,ijl} F_{k,jl} \tag{3}$$

$$Q^{\mathrm{eff}}_{k,ij} = Q^{(0)}_{k,ij} + \alpha^{(21)}_{k,ijl} F_{k,l} + \alpha^{(22)}_{k,ijlm} F_{k,lm} \tag{4}$$

where $F_{k,i}$ and $F_{k,ij}$ are components of the local field and field gradient at site k, $\alpha^{(11)}_{k,ij}$, $\alpha^{(12)}_{k,ijl}$, $\alpha^{(21)}_{k,ijl}$, and $\alpha^{(22)}_{k,ijlm}$ are, respectively, the dipole−dipole, dipole−quadrupole, quadrupole−dipole, and quadrupole−quadrupole polarizabilities at zero frequency of the free molecule, and $\alpha^{(0)}_{k,i}$ and $Q^{(0)}_{k,ij}$ are the corresponding dipole and quadrupole moments of the free molecule. The index k labels all the molecules present in the unit cell. Cartesian indices, which appear twice in a product, are supposed to be summed over. The components $\alpha^{(12)}_{k,ijl}$ and $\alpha^{(21)}_{k,ijl}$ are connected by the relationship $\alpha^{(12)}_{k,ijl} = \alpha^{(21)}_{k,jli}$. Hyperpolarizability effects are neglected.

We also investigated the influence of higher-order multipoles by including permanent octopole $O^{(0)}_{k,ijl}$ and hexadecapole $H^{(0)}_{k,ijlm}$ moments, without the corresponding induced moments and higher-order field derivatives. In the single-point multipole expansion, the local field $\underline{F}_k$ and local field gradient $\underline{\nabla F}_k$ on molecule k are then given by

$$F_{k,i} = (\varepsilon_0 V)^{-1} \sum_l [L^{(11)}_{kl,ij}\mu^{\mathrm{eff}}_{l,j} + L^{(12)}_{kl,ijm} Q^{\mathrm{eff}}_{l,jm} + L^{(13)}_{kl,ijmn} O^{(0)}_{l,jmn} + L^{(14)}_{kl,ijmno} H^{(0)}_{l,jmno}] \tag{5}$$

$$F_{k,ij} = -(\varepsilon_0 V)^{-1} \sum_l [L^{(21)}_{kl,ijm}\mu^{\mathrm{eff}}_{l,m} + L^{(22)}_{kl,ijmn} Q^{\mathrm{eff}}_{l,mn} + L^{(23)}_{kl,ijmno} O^{(0)}_{l,mno}] \tag{6}$$

where $l,k,\ldots$ label the molecules, ϵ_0 is the permittivity of vacuum, V is the volume of the basic simulation box, and $L^{(11)}_{kk',ij}$, $L^{(12)}_{kk',ijl}$, $L^{(21)}_{kk',ijl}$, $L^{(22)}_{kk',ijlm}$, $L^{(13)}_{kk',ijlm}$, $L^{(14)}_{kk',ijlmn}$, $L^{(23)}_{kk',ijlm}$ are components of, respectively, the field-dipole (or Lorentz), field-quadrupole, field-gradient-dipole, field-gradient-quadrupole, field-octopole, field-hexadecapole, and field-gradient-octopole lattice sum tensors, obtained from the corresponding field propagating tensors $T^n(r) = \nabla^n 1/|\underline{r}|$ by the Ewald summation technique,[30] assuming conducting boundary conditions. The lattice sums $L^{(nm)}$ with equal number $n + m$ are connected by simple relationships, for example, $L^{(21)}_{kk',ijl}$ and $L^{(12)}_{kk',ijl}$ are connected by $L^{(12)}_{kk',ijl} = L^{(21)}_{kk',lij}$, where i, j, and l indicate Cartesian coordinate indices. The field gradient contribution of the hexadecapole moments has been neglected. Although the treatment of the octopole and hexadecapole moments is not strictly consistent, the consideration of these moments may give an indication of the convergence behavior of the multipole expansion for the properties under consideration. Therefore, we will report results employing the full sets of multipoles, to which we will refer as the "hexadecapole" (H) approximation, as well as results obtained by neglecting the permanent octopole and hexadecapole moments, that is, putting O, $H = 0$ in eqs 5−6, referred to as the quadrupole (Q) approximation.

The set of linear equations eqs 3−5 can be cast into the form

$$\underline{\underline{\mathscr{X}}} \cdot \underline{\mathscr{F}} = \underline{\underline{\mathscr{L}}} \cdot \underline{\mathscr{M}}^{(0)} \tag{7}$$

Using the symmetry of the matrixes involved, $\underline{\mathscr{F}}$ can be written as a vector $\underline{\mathscr{F}}^T = (\underline{\mathscr{F}}_1, \underline{\mathscr{F}}_2, \ldots, \underline{\mathscr{F}}_N)^T$, where N is the total number of molecules in the simulation box and $\underline{\mathscr{F}}^T_k = (F_{kx}, F_{ky}, F_{kz}, \partial_x F_{kx}, \partial_y F_{kx}, \partial_z F_{kx}, \partial_y F_{ky}, \partial_z F_{ky}, \partial_z F_{kz})^T$. In the Q approximation, $\underline{\mathscr{M}}^{(0)}$ is a N vector of vectors $(\underline{\mathscr{M}}^{(0)}_k)^T = (\mu^{(0)}_{kx}, \mu^{(0)}_{ky}, \mu^{(0)}_{kz}, Q^{(0)}_{kxx}, Q^{(0)}_{kxy}, Q^{(0)}_{kxz}, Q^{(0)}_{kyy}, Q^{(0)}_{kyz}, Q^{(0)}_{kzz})^T$, while in the H approximation, it is a $34N$ vector with additionally the unique (Cartesian) elements of O and H tensors added. Correspondingly, $\underline{\underline{\mathscr{X}}}$ is a $9N\otimes 9N$ matrix build up of N^2 $9\otimes 9$ matrixes $\underline{\underline{\mathscr{X}}}_{kl}$ given by

$$\underline{\underline{\mathscr{X}}}_{kl} = \begin{pmatrix} \delta_{kl}\underline{\underline{I}} - \underline{\underline{L}}^{(11)}_{kl}\cdot\underline{\underline{\alpha}}^{(11)}_l - \underline{\underline{L}}^{(12)}_{kl}\cdot\underline{\underline{\alpha}}^{(21)}_l & -\underline{\underline{L}}^{(11)}_{kl}\cdot\underline{\underline{\alpha}}^{(12L)}_l - \underline{\underline{L}}^{(12)}_{kl}\cdot\underline{\underline{\alpha}}^{(22L)}_l \\ -\underline{\underline{L}}^{(2L1)}_{kl}\cdot\underline{\underline{\alpha}}^{(11)}_l - \underline{\underline{L}}^{(2L2)}_{kl}\cdot\underline{\underline{\alpha}}^{(21)}_l & \delta_{kl}\underline{\underline{I}}^{(6)} - \underline{\underline{L}}^{(2L1)}_{kl}\cdot\underline{\underline{\alpha}}^{(12L)}_l - \underline{\underline{L}}^{(2L2)}_{kl}\cdot\underline{\underline{\alpha}}^{(22L)}_l \end{pmatrix} \tag{8}$$

where the suffix $2L$ means that the two dimensions are linearized in the same way as the field gradient in $\underline{\mathscr{F}}_k$ or the quadrupole moments in $\underline{\mathscr{M}}^{(0)}_k$. $\underline{\underline{I}}^{(6)}$ is a $6\otimes 6$ matrix with elements $I_{ij}{}^{(6)} =$

$\delta_{ij}(\delta_{i4} + \delta_{i5} + \delta_{i6})$. $\overline{\overline{\mathscr{L}}}$ is a matrix consisting of N^2 9⊗9 (Q approximation) or 9⊗34 (H approximation) matrixes $\overline{\overline{\mathscr{L}}}_{kl}$ containing the linearized lattice sum tensors. Equation 7 may be solved by direct inversion of the matrix $\overline{\overline{\mathscr{X}}}$ or by iteration.[26]

The calculation of intermolecular electrostatic interactions using low-order one-center multipole expansions suffers from problems connected with the size and shape of the molecules, especially for larger, nonspherical molecules,[31,32] which can at least partially be overcome by distributing the response properties over the molecule. Although accurate methods for such distribution schemes are available,[33−37] they are generally computationally very expensive. Instead, we used a simple ad-hoc scheme of distributing the electrical properties over a set of intuitively selected parts of the molecule ("submolecules")[38,39] to check for size and shape effects. This approach has been found to correct for the worst deficiencies of the one-point expansion for the prediction of linear and nonlinear susceptibilities in the dipolar approximation of crystals of naphthalene, anthracene, *m*-nitroaniline, and others.[38−40] When this approach is used, the indices *k,l,...* numbering the molecules in the equations above have to be replaced by composite indices *ks,ls,...*, where $s = 1, ..., n_i$ numbers the submolecules of the molecules of sort *i* to which molecule *k* belongs. We shall use the submolecule approach in the same way as in ref 41, by assigning the same part P_i/n_i of each electrical property $P_i = \underline{\mu}_i, \overline{\overline{Q}}_i, \overline{\overline{\alpha}}_i^{(11)}$, and so forth, to each submolecule. Employed in this way, the lower order multipoles create additional higher-order multipole moments at the origin, that is, the *molecular* multipoles are not conserved. For example, the new molecular quadrupole moment $\overline{\overline{Q}}'$ in terms of the original moments $\overline{\overline{Q}}, \underline{\mu}$ is

$$\overline{\overline{Q}}' = \sum_s \overline{\overline{Q}}_s + \sum_s (\underline{\mu}_s \underline{r}_s + \underline{r}_s \underline{\mu}) = \overline{\overline{Q}} + \underline{\mu}/n \sum_s \underline{r}_s + \sum_s \underline{r}_s \underline{\mu}/n \tag{9}$$

where r_s are the coordinates of the submolecules with respect to the molecular origin. However, the additional terms were found to be very small for the molecules considered here (zero for CH and DI) and were thus neglected.

Each second-row atom, together with any hydrogens bound to it, was treated as a separate submolecule, with the center of nuclear charge as the location carrying the electric properties. This leads to 5, 6, 6, and 10 submolecules for THF, CH, DI, and pNA, respectively. The local fields and field gradients are then averaged over the submolecules to obtain the "molecular" fields and gradients.

When the solvent molecules were distributed over more than one submolecule, the computational load becomes very heavy for the larger unit cells; therefore, in these cases, the computations were generally carried out only over part of the trajectory and were then compared with the results of a lower distributed approach computed over the same parts of the trajectory.

To obtain more information on the complex interplay of the employed models and input parameters, we computed several other properties, which are more or less strongly dependent on the intermolecular electrostatic interactions in the liquid and are additionally experimentally accessible and allow thus an easy check of the computed values. The first of these properties is the relative permittivity ϵ_r of the liquids. This property was not used in the derivation of the OPLS-AA force field and may thus serve as an additional test for these parameters.

We computed ϵ_r according to ref 42 by

$$\epsilon_r = \frac{1}{3\epsilon_0 kTV}(\langle \underline{M}^2 \rangle - \langle \underline{M} \rangle^2) + \epsilon_\infty \tag{10}$$

where ϵ_0 is the relative permittivity of the vacuum, *k* the Boltzmann constant, *V* the volume of the simulation unit cell, the brackets denote averaging over the ensemble, and $\underline{M} = \sum_i \underline{\mu}_i^{\text{eff}}$ is the instantaneous dipole moment of the unit cell, with $\underline{\mu}_i^{\text{eff}}$ given by eq 3 and the corresponding local fields and field gradients by eqs 5 and 6. The term $\langle \underline{M} \rangle^2$ is zero for an isotropic liquid; this is usually not the case in molecular simulations due to too short simulation times and/or too small simulation boxes. It was checked that this term was small compared to $\langle \underline{M}^2 \rangle$ and consequently neglected. The term ϵ_∞ is the induced nonorientational relative permittivity, connected with the optical refractive index at high wavelength n_∞ by $\epsilon_\infty = n_\infty^2$. The corresponding linear susceptibility $\lim_{\omega \to 0} \chi^{(1)}(\omega) = \epsilon_\infty - 1$ is computed from[43,44,15]

$$\chi^{(1)}(\omega) \equiv \chi_{ii}^{(1)}(\omega) = (\epsilon_0 V)^{-1} \sum_{kj} \alpha_{k,ij}^{(11),\text{eff}}(\omega) d_{k,ji}(\omega) \tag{11}$$

where the local field tensors $d_{k,ij}$ are given by

$$d_{k,ij}(\omega) = \sum_{k'} D_{ki,k'j}(\omega) = \sum_{k'} \left[\overline{\overline{\mathscr{I}}} - \overline{\overline{\mathscr{L}}}^{(11)} \cdot \overline{\overline{\alpha}}(\omega)/(\epsilon_0 V) \right]^{-1}_{ki,k'j} \tag{12}$$

The matrices $\overline{\overline{\mathscr{L}}}, \overline{\overline{\mathscr{I}}}, \overline{\overline{\alpha}}(\omega)$ are of order 3*Z*, $\overline{\overline{\mathscr{I}}}$ is a generalized unit tensor with elements $I_{ki,k'j} = \delta_{ij}\delta_{kk'}$, while $\overline{\overline{\mathscr{L}}}^{(11)}$ and $\overline{\overline{\alpha}}(\omega)$ have elements $L_{ki,k'j}^{(11)}$ and $\alpha_{k,ij}^{(11),\text{eff}}(\omega)\delta_{kk'}$, respectively. The property $\alpha_{k,ij}^{(11),\text{eff}}(\omega)$ is the corresponding property of the molecule *k* in the liquid, that is, it incorporates the permanent local field effect.[45] For the calculation of ϵ_∞, this generally small effect has been ignored, however. Also, $\chi^{(1)}(\omega)$ has been computed in dipolar approximation only.

Additionally to ϵ_r, we computed the linear and nonlinear *optical* susceptibilities of the pure liquids, again in dipolar approximation, for which experimental values are available in the literature. Equation 11 was employed for the linear susceptibility and

$$\begin{aligned}\chi_{iijj}^{(3)} = (6\varepsilon_0 V)^{-1} \sum_k \; & \times \\ & \gamma_{k,mnop}^{\text{eff}}(-3\omega;\, \omega,\, \omega,\, \omega) d_{k,im}(3\omega) d_{k,ni}(\omega) d_{k,oj}(\omega) d_{k,pj}(\omega) + \\ & \frac{2}{(2\varepsilon_0 V)^2} \sum_{kk'k''} d_{k,mi}(3\omega) d_{k,ni}(\omega) \beta_{k,mno}(-3\omega;\omega,2\omega) \\ & D_{kk',op}(2\omega) L_{k'k'',pq}^{(11)} \beta_{k'',qrs}(-2\omega,\omega,\omega) d_{k'',rj}(\omega) d_{k'',sj}(\omega)\end{aligned} \tag{13}$$

for the nonlinear susceptibility corresponding to third harmonic generation (THG).[44,15] The second term in this expression corresponds to the cascading effect.[15,46] The local field effect on the second hyperpolarizability $\gamma_{k,mnop}^{\text{eff}}(-3\omega;\, \omega,\, \omega,\, \omega)$ has been ignored for CH and DI but not for THF.

We also computed $\chi_{iijj}^{(3)}(-3\omega;\, \omega,\, \omega,\, \omega)$ for the solution of pNA in THF, to check the influence of the cascading terms in relation to the direct term (due to γ). The results will be set in relation to the THG measurements of Meredith and Buchalter in more polar solvents, where the concentration dependence of the apparent γ was interpreted as caused by large cascading effects.[47]

The nonlinear susceptibilities are defined as *perturbative* expansion terms of the Fourier components

of the polarization $P(\omega_\alpha)$, with *external* numerical factors $K^{(n)}_{1,..,n} \equiv K^{(n)}(-\sum_i \omega_i;\omega_1,..\omega_n)$[48]

$$\frac{\underline{P}(\omega)}{\epsilon_0} = \underline{\underline{\chi}}^{(1)}(-\omega;\omega)\cdot\underline{E}_\omega + \sum_{\{\omega_i\}} K^{(2)}_{1,2}\,\underline{\underline{\underline{\chi}}}^{(2)}(-\omega;\omega_1,\omega_2) : \underline{E}_{\omega 2}\underline{E}_{\omega 1} + \sum_{\{\omega_i\}} K^{(3)}_{1,2,3}\underline{\underline{\underline{\underline{\chi}}}}^{(3)}(-\omega;\omega_1,\omega_2,\omega_3)\vdots E_{\omega 3}E_{\omega 2}E_{\omega 1} + ... \quad (14)$$

where $\omega = \sum_{i=1}^{n}\omega_i$ and the numerical factors K depend on the specific NLO process; see, for example, refs 48 and 49. For the two processes considered here, it is $K(-3\omega,\omega,\omega,\omega) = {}^1/_4$ (THG) and $K(-2\omega,\omega,\omega,0) = {}^3/_2$ (EFISH). On the other hand, the Fourier components of the molecular induced dipole moment p are defined as a *Taylor* expansion

$$\underline{p}(\omega) = \underline{\underline{\alpha}}^{(11)}(-\omega;\omega)\cdot\underline{F}_\omega + \frac{1}{2}K^{(2)}_{1,2}\sum_{\{\omega_i\}}\underline{\underline{\underline{\beta}}}(-\omega;\omega_1,\omega_2) : \underline{F}_{\omega 2}\underline{F}_{\omega 1} + \frac{1}{6}\sum_{\{\omega_i\}} K^{(3)}_{1,2,3}\,\underline{\underline{\underline{\underline{\gamma}}}}(-\omega;\omega_1,\omega_2,\omega_3)\vdots\underline{F}_{\omega 3}\underline{F}_{\omega 2}\underline{F}_{\omega 1} \quad (15)$$

where F_ω are the local fields at the molecular site due to the macroscopic fields E_ω.

In the local field and susceptibility calculations, the electric properties of the minimized structure, for which the properties were computed, are assigned to each molecule in the liquid, thus no account is taken for the change of the properties due to the intramolecular geometry changes obtained in the simulation. The rotation matrixes employed to transform from the reference coordinate system to the laboratory system of the MD were computed using the minimization algorithm devised by Kneller.[50]

2.3. Molecular Properties. The electric properties of the single molecules have been reported in part I of this series.[11] In that work, the minimum geometry of pNA has been investigated in the gas phase and in solution phase, by applying different continuum field models at the level of density-functional theory. It was found that the amino group is nonplanar in the gas phase but becomes considerably more planar in solution, with correspondingly pronounced effects on the electric properties. Full planarity was reached in the case of the self-consistent dipolar Onsager reaction field model, while with more sophisticated polarized continuum models (IEFPCM, SCIPCM, BC-COSMO) the molecule is nonplanar, although more planar than in the gas phase. In the latter cases, the planarity increased with basis set size and number of polarization functions and it was not clear if convergence had been achieved with the largest basis set employed (cc-pVTZ and aug-cc-pVDZ). For this work, we have additionally performed an optimization of pNA at the MP2 level, employing the aug-cc-pVDZ basis set and the IEFPCM[51] continuum model for THF as solvent. In this model, the molecule is even less nonplanar than with the DFT models, and consequently, the electric properties are between those of the gas-phase geometry and the DFT/continuum models, as shown in Table 2, which complements Table 3 of ref 11. To compare the effect of the geometries obtained with different continuum models, we used two geometries for the computation of the local field effects on pNA in DI and THF, the one obtained from the B3LYP/Onsager/THF/6-311G** and the MP2/IEFPCM/THF/aug-cc-pVDZ geometry.

In ref 11, a classical averaging of the dipolar electric properties over the torsional and inversion motions was performed and found to have an nonnegligible effect on the dipolar properties of pNA. However, in the present, more approximative work, only the electric properties computed for the optimized

TABLE 3: Computed and Experimental Translational Diffusion Coefficients $D_t/(10^9\ m^2/s)$ of Liquid CH, DI, and THF

liquid	D_t^{calc}	D_t^{exp}
CH	0.83	1.38−1.48[a]
DI (small box)	0.52	1.0[b]
DI (large box)	0.62	1.0[b]
THF	1.93	2.45[c], 3.40[d]

[a] Reference 103. [b] Reference 104. [c] Reference 105. [d] Reference 106.

TABLE 2: Static Electrical Properties of pNA Computed for the Geometries Optimized at MP2/6-311G, B3LYP/OSCRF(ϵ_r = 7)/6-311G**, and MP2/IEFPCM(THF)/aug-cc-pVDZ Levels, Computed at the MP2 (μ − H) and B3LYP ($\alpha^{(12)}$ and $\alpha^{(22)}$) Levels with the Pol Basis Set[a]**

geom.	gas	IEFPCM	OSCRF
μ_x,μ_z	2.378, 0.387	2.514, 0.330	2.799, 0.001
$\alpha^{(11)}_{ii}$	152.06, 105.19, 56.86	156.90, 107,39, 57.54	159.46, 105.03, 56.87
$\alpha^{(11)}_{av}$	104.70	107.28	107.12
β_{xii}	1646.1, −50.0, −50.1	1777.1, −56.9, −54.0	1954.6, −72.7, −62.7
$\beta_{\|\|}$[b]	913.3	988.7	1091.5
γ_{iiii}[c]	144.2, 11.4, 10.7	152.7, 11.1, 12.0	152.9, 11.1, 11.9
γ_{iijj}	−0.4, 5.6, 6.0	−0.9, 6.1, 6.2	−1.8, 6.4, 6.2
γ_{av}	37.8	39.7	39.5
Q_{ii}	−22.5, −19.9, −22.2	−22.2, −19.8, −22.4	−21.1, −20.1, −23.0
O_{iix}	19.5, 3.5, −2.7	21.9, 3.7, −2.8	22.9, 3.5, −3.3
H_{iiii}	−164, −41, −7	−163, −42, −7	−150, −42, −8
H_{ijij}	−34, −30, −9	−34, −31, −9	−33, −33, −8
$\alpha^{(12)}_{x,ii}$	108.7, −7.5, 3.9	110.9, −7.3, 3.9	112.2, −7.5, 3.7
$\alpha^{(12)}_{i,xi}$	“, 13.7, 24.7	“, 14.9, 24.5	“, 14.6, 23.4
$\alpha^{(22)}_{ii,ii}$	1425, 367, 74	1462, 381.8, 75.2	1436, 371, 74
$\alpha^{(22)}_{ii,jj}$	−88, 2, 6	−93, 1, 6	−91, 1, 6
$\alpha^{(22)}_{ij,ij}$	516, 279, 109	529, 283, 111	513, 274, 109

[a] The index *i* runs over *x*, *y*, and *z*, and the double index *ij* runs over *xy*, *xz*, and *yz*. [b] $\beta_{\|\|} = 3/5|\underline{\mu}|\sum_{ij}(\beta_{iij}+\beta_{iji}+\beta_{jii})\mu_j$. [c] γ in 10^3 au, all other units in atomic units.

geometries were used; the dependence on the internal degrees of freedom was not taken into account.

The properties for the solvent molecules CH, DI, and THF were also taken from ref 11. Except for the PV of THF, vibrational contributions were taken into account, the ZPVA for all computations, the PV contributions for all static computations. The PVs of THF are probably divergent according to ref 11.

3. Results and Discussion

3.1. Pure solvents: Local Fields, Relative Permittivities, and Optical Susceptibilities. Liquid 1,4-dioxane seems not to have been simulated previously with the OPLS-AA parameters. To perform the usual tests of the employed force field, we conducted separately a NPT simulation of the liquid with 54 molecules in the unit cell (200 ps) and a 2 ns single molecule simulation to compute the vaporization enthalpy $\Delta_{vap}H^0$ and the density ρ_{298K}, using the same procedures as employed by Jorgensen et al.[21−22] in the derivation of the OPLS-AA parameters; the results are $\Delta_{vap}H^0 = (39.8 \pm 2)$ kJ/mol and $\rho_{298K} = (1.018 \pm 0.018)$ g/cm^3, which compare reasonably well with the corresponding experimental values $\Delta_{vap}H^0 = 38.66$ kJ/mol[52] and $\rho_{298} = 1.02687$ g/mL.[53]

As an additional check of the OPLS-AA potential for DI, we computed the energy difference between two stable conformers of 1,4-dioxane, the chair and the 1,4-twist-boat structure, which was found to be 38.4 kJ/mol, in satisfactory agreement with the corresponding energy difference of 31.2 kJ/mol computed at the MP2/6-31G* level.[54]

The computed translational diffusion coefficients D_t together with experimental data are given in Table 3. The values obtained for the two DI boxes show that the box size has a nonnegligible influence on D_t; among all the computed properties here, this is the only occasion where this happens. Although comparison with the experimental values is not very good in terms of the absolute values, the trends among the three solvents are predicted correctly. Uncertainties in the experimental values, as evidenced by the large spread in the THF values and the possibly remaining dependence of the computed values on the box size, may explain part of the absolute deviations.

The liquid structure of THF and DI has been determined by X-ray scattering measurements by Takamuku et al.,[55,56] while Farman et al. measured the neutron diffraction of C_6D_{12}.[57] To compare the simulated liquids with the experimental results, we computed for DI and THF the molecular radial distribution function (MRDF) $D(r)$, following ref 58, by

$$D(r) = 4\pi\rho \sum_{ij} \bar{K}_i \bar{K}_j [g_{ij}(r) - 1] r^2 \qquad (16)$$

where ρ is the number density, i, j label the atoms in the molecule, $g_{ij}(r)$ is the intermolecular radial distribution function of atoms i and j, and $\bar{K}_i$ is the averaged effective number of diffracting electrons of atom i computed in the Warren−Krutter−Morningstar approximation[59]

$$\bar{K}_i = \frac{1}{s_2 - s_1} \left(\sum_m Z_m\right) \int_{s_1}^{s_2} \mathrm{d}s \, \frac{f_i(s)}{\sum_m f_m(s)} \qquad (17)$$

where Z_m is the number of electrons in atom m and $f_i(s)$ is the atomic scattering factor, taken from ref 60. For liquid CH, we calculated, following ref 57

$$d_L(r) = 4\pi r\rho \sum_{ij} b_i b_j [g_{ij} - 1] = 4\pi r\rho [0.111 g_{CC}(r) + 0.445 g_{CH}(r) + 0.444 g_{HH}(r)] \qquad (18)$$

where the b_i are neutron scattering factors. No further corrections have been made for the difference of D and H.

In parts a−c of Figure 2, we compare the functions with the corresponding experimental radial distribution functions given by Takamuku et al.[55,56] and Farman et al.[57] (at 27 °C), the latter corrected for intramolecular scattering, assuming either a boat or a chair configuration. It can be seen that in all three cases the simulated radial distribution functions reproduce the positions of the maxima r_{max} and minima r_{min} in the intermolecular region very well but overestimate the corresponding absolute values of the MRDFs considerably, that is, the simulated liquids are ordered too strongly.

Together with the results of previous simulation work on THF and CH using the OPLS-AA potential,[23] our simulation results show that this potential is able to reproduce fundamental properties of the pure liquids reasonably well, probably as good as can be expected considering the simple form of the potential employed.

Using the methods described in section 2, we computed the average molecular local fields and field gradients in the pure liquids CH, DI, and THF, as well as their relative permittivities, linear optical susceptibilities, and nonlinear THG susceptibilities, for which experimental values are available.[61−63] They allow a check of the parameters employed in the molecular simulations, the computed properties, and the electrostatic model employed. In Table 4, we list the computed fields and field gradients and the static relative permittivities for all three liquids as well as the first susceptibilities $\chi^{(1)}(\omega)$, $\chi^{(1)}(3\omega)$, and the THG susceptibilities $\chi^{(3)}(3\omega; \omega, \omega, \omega)$ of the liquids at $\omega = 0.023896$ au ($\lambda = 1907$ nm), together with available experimental values. All the values have been computed in the one-point expansion approach, using the quadrupolar approximation for the fields and ϵ_r and the dipolar approximation for the optical properties. While the one-point "hexadecapolar" approximation did not change the values appreciably and are therefore not shown, a higher distributed approach did have an effect on some properties of THF, as will be mentioned below, but not on those

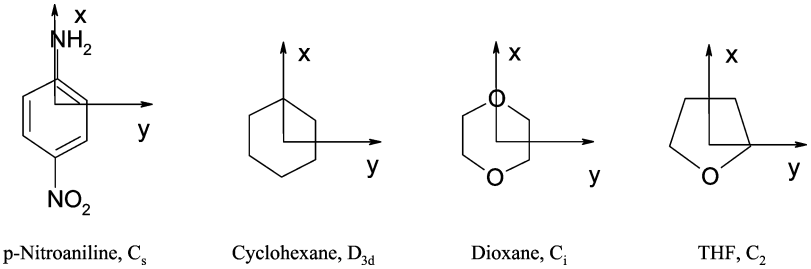

p-Nitroaniline, C_s Cyclohexane, D_{3d} Dioxane, C_i THF, C_2

Figure 1. Structural formulas, molecular coordinate systems, and symmetry groups of *p*-nitroaniline (pNA), cyclohexane (CH), 1,4-dioxane (DI), and tetrahydrofuran (THF).

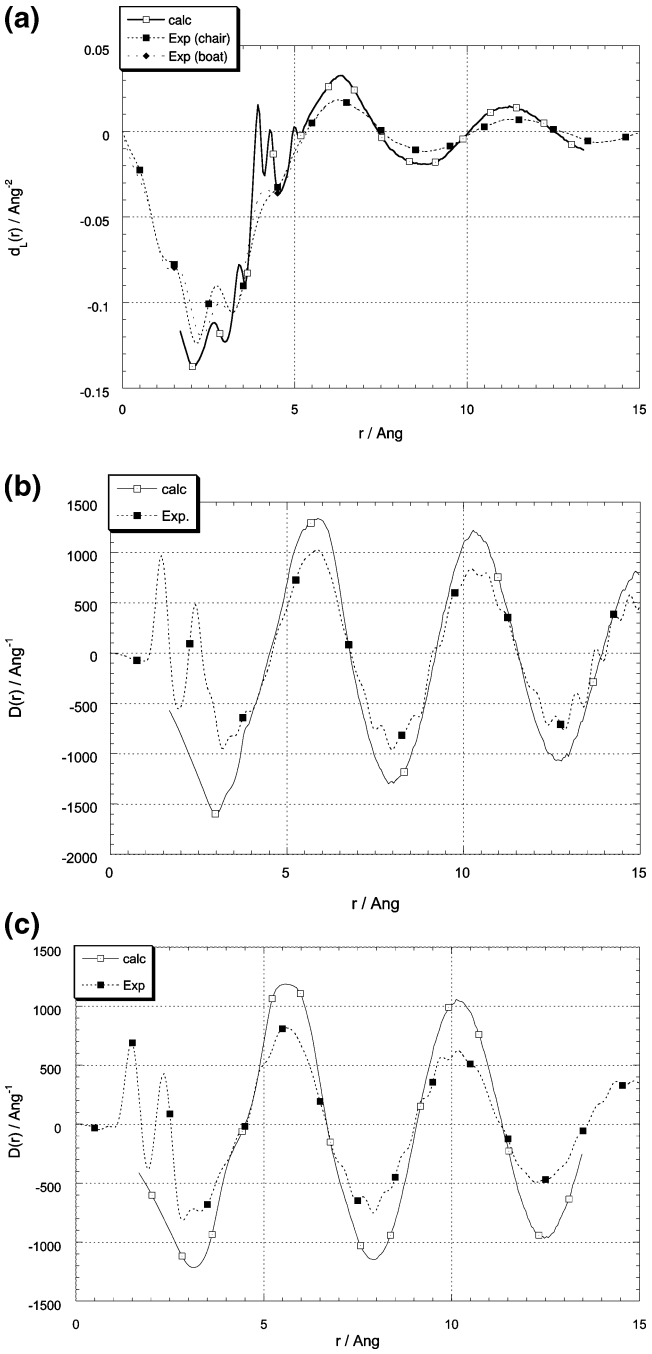

Figure 2. Computed and experimental radial distribution functions $d(r)$ for (a) cyclohexane, (b) 1,4-dioxane, and (c) tetrahydrofuran. In the experimental curve for CH, the intramolecular part has been subtracted,[57] assuming either a boat or a chair configuration for the molecule.

of DI and CH. Computations using the larger unit cell for DI yielded virtually the same results.

The average local fields and field gradients obtained for the systems investigated here reflect the dominant multipolar moments of the constituting molecules. In THF, the permanent dipole moment creates a considerable local field component in the direction of the molecular dipole moment, as expected. In DI, the local field gradients, mainly due to the quadrupole moments, are quite large in comparison with the other two liquids, but still so small as to have a nearly negligible effect on the dipolar (hyper)polarizabilities, as shown below.

The relative permittivities, with the exception of liquid THF, and the optical first susceptibilities are quite well reproduced by the calculations, with generally not more than ±5% deviations from the experimental values. Note that this translates into ±1−2% difference for the refractive indices. An interesting feature is found for liquid DI, for which the experimental static $\epsilon_r - 1$ value is larger than the optical susceptibility $\chi^{(1)}(\omega)$ at frequencies in the UV−vis range. This is rather unusual for a nonpolar liquid, because generally the frequency dispersion effect on the polarziabilities leads to the opposite ordering of static and optical susceptibilities. One possible explanation is to assume that a substantial part of the DI molecules in the liquid adopts a dipolar boat or twist-chair conformation,[64] so that on average the DI molecules in the liquid carry a nonvanishing permanent dipole moment, estimated from dielectric measurements to be as large as ∼0.5 D.[64] This dipole moment would then lead to an orientational contribution to ϵ_r, which would be absent in the optical susceptibilities. On the other hand, ab initio calculations on the isolated molecule[54] have shown that the chair conformer is about 30−40 kJ/mol more stable than the energetically next higher conformers. Our calculations suggest an alternative explanation.

We note first that, in the susceptibility calculations, contrary to the simulations, the DI molecules in the liquid are considered to be rigid, carrying the electric properties of the nonpolar chair conformer. Nevertheless, the simulated susceptibilities reproduce both the static and frequency-dependent experimental values quite well. The difference between static and optical susceptibilities in our case is due to the comparably large pure vibrational contributions to $\alpha^{(11)}$, which contribute to ϵ_∞, but not to $\chi^{(1)}(\omega)$ for optical frequencies ω. Additionally, the small permanent fields increase ϵ_r further. However, for ϵ_r, the quadrupolar approximation was adopted, while for ϵ_∞ and $\chi^{(1)}(\omega)$ we used the dipolar approximation and the two set of values are therefore not strictly comparable.

Our computed value of the relative permittivity of THF underestimates the experimental value by 30%. Similar underestimations of ϵ_r have been found for ethanol[65] using OPLS-AA parameters in unpolarized simulations. Our value is also similar to the value which Richardi et al.[66] obtained for THF, using the hypernetted chain approximation of the molecular Ornstein−Zernike theory, treating THF as a rigid molecule, employing the OPLS-UA parameters, and taking the polarizability into account in the framework of a self-consistent mean-field theory. They speculate that the underestimation may be due to a neglect of dipole fluctuations orthogonal to the permanent dipole axis and/or the use of a one-point polarizability instead of atomic and bond polarizabilities. In our simulations, the first point is automatically taken into account and the second point could at least roughly be tested by the five submolecule approach, for which we get $\epsilon_r = 5.74$ after averaging over 70 ps and neglecting the $\langle \underline{M} \rangle^2$ term in eq 10, which is rather large due to the small averaging time period. This value is about 10% larger than the one obtained in the one-point approach averaged over the same part of the trajectory, $\epsilon_r = 5.20$. Although this enhancement is in the right direction, it is still too small. Better agreement would probably require a more accurate (polarizable) force field in the molecular simulation and/or a more accurate distribution scheme for the electrical properties, as those advocated by LeSueur and Stone[33,34] or Ángyán et al.[35,31]

To compute the THG signal of THF, the molecular (hyper)-polarizabilities were first recomputed in the permanent local field found for the liquid in the one-point approximation, ignoring the gradient contribution, which is small. The average properties in the local field are, at the static MP2 level: $\mu^{\text{eff}} = 0.87$ au (0.73 au), $\alpha_{\text{av}}^{(11),\text{eff}} = 51.82$ au (51.86 au), $\beta_{||}^{\text{eff}} = -18$ au

TABLE 4: Computed Values of Average Local Fields $F_{i=x,y,z}/10^9$ V/m, Field Gradients $F_{ii=xx,yy,zz}$, $F_{ij=xy,xz,yz}/10^{18}$ V/m^2 in Quadrupolar (Q) Approximation, Relative Permittivities ϵ_r, and Its Induced Contribution $\epsilon_\infty \equiv \chi^{(1)}(0) + 1$, as Well as First $\chi^{(1)}(\omega)$, $\chi^{(1)}(3\omega)$, and Third Order (THG) $\chi^{(3)}(3\omega) \equiv \chi^{(3)}(-3\omega; \omega, \omega, \omega)/(10^{-24}$ m^2/V^2) Susceptibilities at $\omega = 0.023896$ au of Liquid CH, DI, and THF at $T = 298$ K

	CH		DI		THF	
F_i	0.0, 0.0, 0.0		0.0, 0.0, 0.0		1.3, 0.0, 0.0	
F_{ii}	0, 0, 0		−12, 12, 0		−4, 4, 0	
F_{ij}	0, 0, 0		0, 4, 0		0, 0, 0	
	calc.	exp.	calc.	exp.	calc.	exp.
ϵ_r	2.040 ± 0.001	2.025[a]	2.333 ± 0.003	2.209[b]	5.64 ± 0.1	7.58[c]
ϵ_∞	2.040 ± 0.001		2.177 ± 0.003		1.9746 ± 0.0001	
$\chi^{(1)}(\omega)$	1.027 ± 0.001		1.027 ± 0.004	0.9842[d]	0.9760	
$\chi^{(1)}(3\omega)$	1.047 ± 0.001	1.028[b,e]	1.047 ± 0.003	1.0123[d]	0.9951	0.9760[f]
$\chi_{iiii}^{(3)}(3\omega)$	327.3 ± 0.5	325 [g,h]	360.1 ± 2.0	277[d,h], 320[i,h]	286.2 ± 0.6	292[f,h]

[a] Reference 107, 293 K. [b] Reference 108. [c] Reference 109. [d] Reference 62. [e] $\omega = 0.07737$ au ($\lambda = 589$ nm). [f] Reference 67. [g] Reference 61. [h] Experimental $\chi^{(3)}$ values were rescaled with the calibration value of ref 68. [i] Reference 63.

(−42 au), and $\gamma_{av}^{eff} = 9631$ au (9681 au), where the corresponding gas-phase properties from ref 11 are given in parentheses. The values show that the local field has a large effect on μ and β, but only a very small influence on $\alpha^{(11)}$ and γ, which determine $\chi^{(3)}$.

We also computed the properties of DI including the effect of the average local field gradients obtained for the simulated structures. At the MP2 level, these field gradients *decrease* the polarizabilities ($\alpha_{av}^{(11)} = 56.43$ au, −0.4% compared with the field free value) and second hyperpolarizabilities ($\gamma_{av} = 11\,221$ au, −3.5%). Due to the smallness of the effects, the gas-phase values were used for the calculation of the susceptibilities of liquid DI.

The computed THG signals of liquid CH and THF match the experimental values[61,67] closely, if the latter values are rescaled with the most recent calibration factor for THG measurements, determined by Bosshard et al.[68] The cascading contribution to $\chi^{(3)}$ for THF is negligibly small (lower than 1%). The computed THG susceptibility of DI, however, is 10−25% larger than the two available experimental values,[62,63] which differ by over 10% among each other. Using the *in-field gradient* properties instead of free molecule properties would lead only to a decrease of 3−5%. A possible explanation for the difference could be the presence of a substantial amount of different conformers in the liquid. In ref 11, we reported the static (hyper)-polarizabilities for the two other conformers of 1,4-dioxane, which are local minima on the potential surface according to the computations of Chapman and Hester,[54] namely, the 1,4-twist-boat (14TB) and the 2,5-twist-boat (25TB) conformers, after geometry optimization at the DFT/B3LYP level with the 6-311G** basis. The average properties at the SCF/Pol level found for the 14TB (symmetry D_2) were as follows: $\alpha_{av}^{(11)} = 52.13$ au (−2%), $\gamma_{av} = 5720$ au (−22%), and for 25TB (symmetry C_2): $\mu = 0.7$ au, $\alpha_{av}^{(11)} = 52.40$ au (−2%), $\beta_{||} = -98$ au, and $\gamma_{av} = 6355$ au (−10%), where the numbers in parentheses indicate the differences to the chair conformer. These values show that a substantial amount of the nonpolar 14TB conformer present in the liquid could in fact lead to a lower $\chi^{(3)}$ value. However, as already mentioned, the two conformers are both predicted to be more than 30 kJ/mol higher in energy than the chair conformer, which corresponds to more than 10 times the thermal energy RT at room temperature, which makes the presence of a substantial amount rather unlikely. Clearly, there are other possible sources of error, such as too low a correlation level, basis set and geometry effects, effects due to the flexibility of the molecules in the liquid, and so forth. Overall, however, taking into account the approximations made and the uncertainties in the experimental values reflected in the disparity between the available data, we believe that the agreement between computed and experimental values is reasonably good.

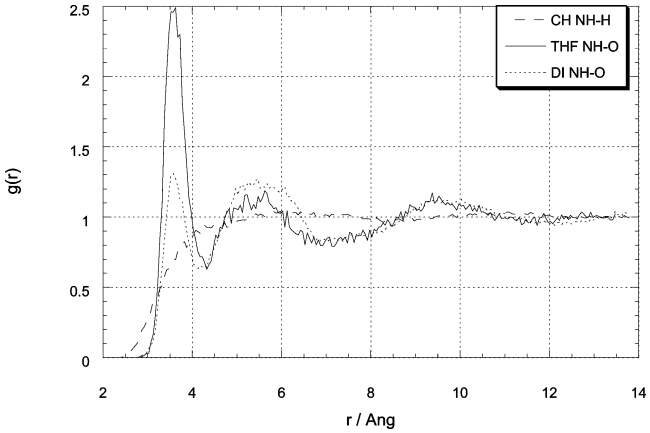

Figure 3. Radial distribution functions (RDFs) for pNA/THF and pNA/DI for the amino hydrogens (NH) and the oxygen atom in the solvent molecules (OS). For comparison, the RDFs of NH and the hydrogen atom in CH are also shown.

We emphasize that the calibration factor employed for the experimental results plays a decisive role in the good agreement between computed and experimental values found here; using instead of the value determined by Bosshard et al.[68] the one employed originally by Kajzar et al.[61,62] and Cheng et al.,[63] which was obtained by Buchalter and Meredith,[69] or the one determined by Mito et al.[70] leads to pronounced disagreement with our computed values.

3.2. Solutions: Local Fields, Relative Permittivities, and Effective (hyper)Polarizabilities of pNA. Before going into the details of the electrostatic computations for the solutions of pNA, we report some results of the molecular simulations. The translational diffusion coefficient of the solvent molecules is only affected little by the solute for CH and DI, the values are 0.65×10^9 s/m^2 and 0.77×10^9 s/m^2 for CH and DI, respectively, compared with 0.62×10^9 s/m^2 and 0.83×10^9 s/m^2 in the pure solvents. The value of D for THF, however, is substantially reduced in the solution (1.46×10^9 s/m^2 vs 1.93×10^9 s/m^2).

The radial distribution functions (RDFs) for pNA/THF and pNA/DI for the amino hydrogens (NH) and the oxygen atom in the solvent molecules (OS) (see Figure 3) show a strong first peak at 1.7−1.8 Å, which can be interpreted as a hydrogen bond between the two atoms. Huyskens et al.[71] deduced the existence

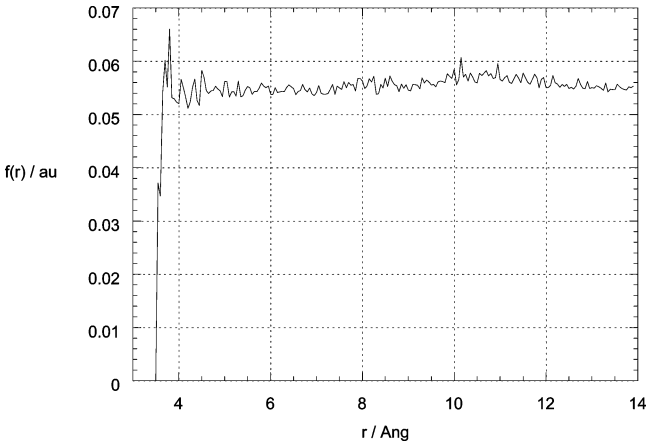

Figure 4. Dipole distribution function $f(r)$ of pNA in 1,4-dioxane.

TABLE 5: Average Local Fields $F_x/10^9$ V/m, in Quadrupolar (Q) and "hexadecapolar" (H) Approximation for pNA in CH, DI, and THF, Obtained with Different Submolecule Distributions m/n[a] and the Local Field Computed Using the Onsager Approximation

		CH		DI		THF	
m/*n*		Q	H	Q	H	Q	H
1/1	OSCRF	1.76	0.48	3.27	1.24	3.35	1.63
1/10	OSCRF	1.08	1.00	2.91	2.91	2.78	2.83
1/10	IEFPCM	0.96	0.90	2.76	2.77	2.66	2.73
Onsager approximation							
F_x		1.50		3.05		3.26 ($\epsilon_r = 7.58$) 2.99 ($\epsilon_r = 5.64$)	

[a] $n = 1$, 10 for pNA, $m = 1$ for the solvent molecules.

of solute−solvent H-bonds for pNA in DI from a comparison of experimental solubilities of pNA and *N*,*N*-dimethyl-pNA.

An explanation advanced previously for the apparent polarity of 1,4-dioxane for dipolar solutes is that the dipolar solute induces a transition of the nonpolar chair form of dioxane to a polar conformation, so that the solutes feel a "microscopic" relative permittivity which is larger than the bulk value.[10,72] To test this supposition, we checked if the high polarity of pNA leads to an increase of dioxane molecules with a polar configuration in the solvent shells surrounding the solute in the pNA/DI solution. Thus, we computed a dipole distribution function $f(r)$ by

$$f(r) = \int_r^{r+\Delta r} |\underline{\mu}(r')| \mathrm{d}r'/N(r) \tag{19}$$

where r is the distance from the center of mass (COM) of the pNA molecule, $\mu(r)$ is the dipole moment at the COM of a DI molecule computed with the partial charges used in the simulation, Δr is a sampling interval, and $N(r)$ is the number of DI molecules with their center of mass in the shell $[r, r + \Delta r]$. This function, computed with a sampling interval of 0.05 Å, is shown in Figure 4. It shows that the average dipole moment of the solvent molecules is very small and nearly independent of the distance to the solute, so that the simulation results do not support the idea of an increased solvent polarity due to conformational changes, induced by the high solute polarity.

The local fields and field gradients on pNA in the different solutions computed using different distribution schemes *m*/*n*, where *n* denotes the number of submolecules on pNA and *m* those on the solvent molecules, are shown in Table 5. The average fields and field gradients on the solvent molecules (not shown) are practically the same as those found for the pure solvents, which means that the concentration of pNA is too small to change the average local field on the solvent molecules.

The data show that, for the one-point expansion ($m/n = 1{:}1$), there is a large difference between the Q and the H approximation, for example, F_x, the field component in the direction of the dipole moment, is in the H approximation only about 25−50% as large as in the Q approximation. On the other hand, in the $n = 10$ approach for pNA, the values obtained in the H approximation are very similar to those obtained in the Q approximation. We also used the distributions $m/n = 5$, 6:10, however, in these cases, the iterative method did often not converge. This may be ascribed to the so-called "polarization catastrophe", which happens if two polarizable centers get too close to each other.[73,74] Nevertheless, using only the converged calculations, the differences in the fields and field gradients compared with the $m/n = 1/10$ distribution were generally similar to those found for the $n = 1$ and $n = 5$ distributions of pure THF: about 10−20% larger in magnitude, which we feel is too small to be considered a real distribution effect in view of the crude distribution method.

Only for pNA, therefore, do we find a considerable influence of the specific molecular shape and size on the local fields. This is not very surprising, because this molecule has the largest spatial extension, the strongest deviation from spherical shape, and the largest polarizabilities among the molecules considered here, three conditions which are known to lead to more pronounced size and shape effects. More insight can be gained by examining the contribution of the single multipole terms to the fields and field gradients in eqs 5 and 6, according to

$$\underline{F}_k^{(n)} = (\epsilon_0 v)^{-1} \sum_{l \neq k} L_{kl}^{(1n)} | M_l^{(n),\mathrm{eff}} \tag{20}$$

and a similar equation for the field gradients. Here, $M^{(n)} = \mu$, Q, O, H for $n = 1, 2, 3, 4$, and the | denotes *n*-fold contraction. Note that $\underline{F}_k^{(1)}$, $\underline{F}_k^{(2)}$, and the respective gradient terms do not necessarily vanish if the corresponding *permanent* dipoles and quadrupoles, respectively, are zero, because the effective moments contain indirect contributions from both permanent moments, compare eqs 3 and 4. On the other hand, $\underline{F}_k^{(3)}$, $\underline{F}_k^{(4)}$, vanish if the corresponding permanent multipole moments are zero in the approximation adopted here. To examine the influence of the different contributions of the *polarization* on the fields, we performed additional computations where either all polarizabilities were put to zero, thus probing only the fields due to the permanent multipoles, or the dipole−dipole polarizabilities were retained and the higher-order polarizabilities were zero.

The results of the analysis are shown in Table 6 for F_x of pNA. It can be seen that the field decrease from the Q to the H approximation in the fully polarized one-point expansion is nearly entirely due to the octopole moments, whose contribution to F_x is large in all three solvents, much larger than the hexadecapole and quadrupole contributions. In the two solvents without permanent octopole moments, CH and DI, this large field component is then entirely a reaction field due to the permanent octopole moments of pNA and with an opposite sign as the dipolar contribution. This is at least an unusual pattern for a strongly dipolar molecule as pNA. If the response properties of pNA are distributed over 10 submolecules, then the pattern becomes much more reasonable: now the dipolar and/or quadrupolar components of the field are much larger than the higher-order field components. Additionally, there is a general decrease of the dipolar contribution, and an increase of

TABLE 6: Average Contributions F^{μ}, F^{Q}, F^{O}, and F^{H} of Different Multipoles to F_x of pNA in CH, DI, and THF, Computed with eq 21, without Any ($\alpha = 0$), with Only Dipole−Dipole ($\alpha^{(11)} \neq 0$), and with All ($\alpha \neq 0$) Polarizabilities Included

	1/1		1/10		
n/*m*	$\alpha = 0$	$\alpha \neq 0$	$\alpha = 0$	$\alpha^{(11)} \neq 0$	$\alpha \neq 0$
			CH		
F_x^{μ}	0.03	1.76	0.03	0.77	1.08
F_x^{Q}	−0.01	0.00	−0.01	−0.01	−0.01
F_x^{O}	0.00	−1.28	0.00	−0.06	−0.06
F_x^{H}	0.00	0.00	0.00	−0.01	−0.01
			DI		
F_x^{μ}	0.04	2.31	0.04	0.95	1.31
F_x^{Q}	1.10	0.96	1.53	1.38	1.61
F_x^{O}	−0.00	−1.99	−0.00	−0.05	−0.08
F_x^{H}	−0.03	−0.04	0.11	0.11	0.08
			THF		
F_x^{μ}	1.10	3.05	1.56	1.96	2.33
F_x^{Q}	0.24	0.29	0.51	0.41	0.44
F_x^{O}	0.04	−1.75	0.12	0.03	0.04
F_x^{H}	0.00	0.03	0.02	0.02	0.02

the quadrupolar contribution, of more than 100% for the DI solution and a smaller one for the THF solution. For DI, the quadrupole field is then the largest contribution to F_x, while for CH and THF, the dipolar field becomes dominant. This is in line with what one would expect for a dipolar solute in a quadrupolar (DI), nonpolar (CH), or dipolar (THF) solvent. Thus, only the $n = 10$ distribution for pNA leads to physically reasonable results, in contrast to the one-point approximation.

Comparison of the nonpolarized and polarized fields for the $n = 10$ distribution shows that the polarization enhances the dipolar field component strongly, while the quadrupolar component is mainly due to the permanent quadrupoles. This means that the field dominating quantities are the dipoles, quadrupoles, and dipole−dipole polarizabilities $\alpha^{(11)}$.

It is interesting to compare the obtained results with those of dielectric continuum models, which are used to extract molecular properties from experimentally determined susceptibilities; see, for example, refs 75 and 76. In these models, the molecule is supposed to reside in a cavity surrounded by a continuous dielectric. The shape and the dimensions of this cavity are generally ill-defined but determine to a large extent the predicted properties. One of the more accurate representatives of these models is the ellipsoidal Onsager model in dipolar approximation, where the reaction field for a molecule in an ellipsoidal cavity of half-axes a_x,a_y, a_z and with the dipole along axis z is given by

$$E_z^R = f_{zz}^{R0}[1 - f_{zz}^{R0}\alpha_{zz}^{(11)}]\mu_z^0 \tag{21}$$

with

$$f_{zz}^{R0} = \frac{3\kappa_z(1-\kappa_z)(\epsilon_r - 1)}{4\pi\epsilon_0 a_x a_y a_z[\epsilon_r - \kappa_r(\epsilon_r - 1)]} \tag{22}$$

where k_i are depolarization factors; see, for example, ref 75. For dipolar solvents, the relative permittivity ϵ_r is the experimental quantity. For 1,4-dioxane, however, an empirically determined "microscopic" permittivity is usually used for ϵ_r, with a value of 6−7, to account for the apparent higher "polarity" of this solvent.[7,8] The values obtained for the reaction field F_x of pNA in the Onsager model are given in the last row of Table 5, using, following Wortmann et al., (a_x, a_y, a_z) = (5.1, 3.8, 2.1) Å, obtained from van der Waals radii plus an empirical increment of 0.4 Å,[8] $\epsilon_r = 2.025$, 6, and 7.58 for CH, DI, and THF. The dimensions of the cavity were estimated for the planar pNA molecule, and we thus employed the properties computed for the planar OSCRF geometry for the Onsager model. For pNA/CH, the Onsager prediction is about 50% larger than that of the discrete local field model, but for pNA/DI and pNA/THF, the values are quite similar to those obtained in the discrete local field model with the $m/n = 1{:}10$ distribution, although the field in THF is predicted to be larger than that in DI. If the simulated value for ϵ_r of THF (5.64, see Table 4) is used instead of the experimental value, then the value predicted by the Onsager model is in even better agreement with the discrete model prediction.

Thus, for pNA, we find that with a carefully chosen set of parameters it is possible to obtain similar values with the Onsager continuum model as with the supposedly more accurate discrete model, at least for the medium polar solvents THF and DI. One notes also that the dipolar ellipsoidal Onsager model, as employed here, seems to be able to take into account the effect of the quadrupoles, both permanent and induced. Whether this is an accidental coincidence or a general feature remains to be investigated, however.

To quantify the effect of the local field on the hyperpolarizabilities and the EFISH signal of pNA, we recalculated the electric properties with the OSCRF and the IEFPCM-optimized geometries with the different external fields added to the Hamiltonian. Preliminary calculations showed that the local field gradients were too small to have an appreciable influence on the properties and were thus neglected. To be comparable with the gas-phase computations in ref 11 and in Table 2, static properties were computed at the MP2 level with the Pol[77] basis set. The frequency dispersion of all properties at $\omega = 0.04282$ ($\lambda = 1064$ nm) and for pNA/DI, at $\omega = 0.02389$ ($\lambda = 1907$ nm), was computed with the random phase approximation (RPA) with Pol. To check on correlation effects on the dispersion, the dominant component of the first hyperpolarizability $\beta_{xxx}(-2\omega; \omega, \omega)$ was computed at the CC2 level with a basis set based on Dunning's double-ζ valence set, augmented with d functions ($\alpha = 0.2$) on C, N, and O and with p functions on H ($\alpha = 0.1$), abbreviated by D95V(p,d). With the IEFPCM geometry and the field obtained for DI solution, the dispersion obtained at $\omega = 0.0428$ ($\lambda = 1064$ nm) ($\beta_{xxx}(-2\omega; \omega, \omega)/\beta(0;0,0)$ = (3247.6 au)/(2046.9 au) = 1.587) was similar to that without field ($\beta_{xxx}(-2\omega; \omega, \omega)/\beta(0;0,0)$ = (3079.3 au)/(1960.2 au) = 1.571), thus the other field/geometry combinations were not checked out at the CC2 level. The reason for this small change in dispersion may be due to insufficient basis set flexibility.

Table 7 shows dipole moments μ, average polarizabilities α_{av} and second hyperpolarizabilities γ_{av}, the parallel component of the first hyperpolarizability $\beta_{||}$ and the two dominant components β_{xxx}, γ_{xxxx} for pNA at the static MP2/Pol level subject to the permanent local field obtained in the three solvents. Also shown are the scaling factors for β and γ, obtained at the RPA/Pol level. Comparison with the field-free properties in Table 2 shows that the field has a strong effect on β, a sizable effect on μ and γ, and a small effect on α. The same pattern has been found in other occasions.[15,40,41,45] Properties obtained for the IEFPCM-optimized geometry are between 0% and 10% smaller than those computed for the OSCRF-optimized geometry. As expected from the similar values of the local field, the properties of pNA in THF and DI are also quite similar.

TABLE 7: Static Electric Properties of pNA in the Local Fields Obtained in CH, DI, and THF Solutions, Computed at the MP2/Pol Level, and Scaling Factors $S(\omega) = \beta(-2\omega;\omega,\omega)/\beta(0;0,0)$, $\gamma(-2\omega;\omega,\omega,0)/\gamma(0;0,0,0)$, Obtained at the RPA/Pol Level[a]

solvent	CH	DI		THF	
geometry	IEFPCM	IEFPCM	OSCRF	IEFPCM	OSCRF
μ	2.985	3.407	3.739	3.573	3.711
α_{av}	107.32	111.09	111.45	110.05	111.30
$\beta_{xxx}(0;0,0)$	2124.0	2758.1	2848.5	2771.9	2932.8
$S(0.0428$ au)	1.3845	1.4180	1.4463	1.4195	1.4349
$\beta_{\|\|}(0;0,0)$	1199.0	1589.5	1709.1	1593.4	1688.1
$S(0.0428$ au)	1.4267	1.4532	1.4805	1.4518	1.4696
$S(0.0239$ au)		1.1140	1.1202		
$\gamma_{xxxx}(0;0,0,0)$	164.5	213.0	205.3	200.0	203.7
$S(0.0428$ au)	1.5012		1.6454		
$\gamma_{av}(0;0,0,0)$	41.4	50.3	48.5	47.6	48.3
$S(0.0428$ au)	1.3878		1.5169		
$S(0.0239$ au)			1.1221		

[a] γ in 10^3 au, all other units in atomic units.

To relate with experimental values, the electric properties were used to compute the EFISH signal $\langle\gamma\rangle_E$ and the property $\langle\beta_{ZZZ}\rangle$ related to the hyper-Rayleigh (HRS) scattering signal. The EFISH signal, as obtained from the experimental susceptibility in the Onsager continuum approximation, is defined as

$$\langle\gamma\rangle_E = \frac{\mu^0\beta_{||}}{3kT} + \gamma_{av} \tag{23}$$

where μ^0 is the dipole moment of the *isolated* molecule, while $\beta_{||}$ and γ_{av} are the properties of the *solvated* molecule.[75,78] The property $\langle\beta_{ZZZ}\rangle$ related to HRS was computed according to the general equation given by Bersohn et al.[79] using the components of the solute β tensor. Similarly as in part I,[11] frequency dispersion as well as correlation effects on the dispersion were taken into account by scaling factors, considering that the absolute CC2 values probably overestimate the electric properties, while the frequency dispersion at the CC2 level is more accurate than the one computed at the RPA level. Thus, the properties $\beta_{||}(-2\omega;\omega,\omega)$ at $\omega = 0.0428$ au were computed from

$$\beta_{||}(-2\omega;\omega,\omega) \approx \beta_{||}(0;0,0)S_{xxx}(\mathrm{CC2})\frac{S_{||}(\mathrm{RPA})}{S_{xxx}(\mathrm{RPA})} \tag{24}$$

where the S_k(Meth.) are scaling factors given by S_k(Meth.) = $\beta_k(-2\omega;\omega,\omega)$(Meth.)/$\beta_k(0;0,0)$(Meth.), with $S_{xxx}(\mathrm{CC2}) = 1.58$. At $\omega = 0.0239$ au, the dispersions at the CC2/D95V(p,d) level and the RPA/Pol level are very similar, therefore only the RPA/Pol dispersion was taken into account. A similar procedure was employed for $\langle\beta_{ZZZ}\rangle$, with $\beta_{||}$ replaced by the combination of components computed according to ref 79. The property $\gamma_{av}(-2\omega;\omega,\omega,0)$, which makes only a small contribution to $\langle\gamma\rangle_E$, was computed with additional approximations: S_{xxx}(CC2) for $\omega = 0.0428$ au was approximated from zero field computations of ref 11 as 1.80 and the RPA/Pol scaling factor computed for DI for the OSCRF geometry was employed for all computations in THF and DI solvent.

Table 8 shows computed and comparable experimental values of $\langle\gamma\rangle_E$ and $\langle\beta_{ZZZ}\rangle$. Some preliminary remarks are in order to justify the compilation of the experimental values. Comparison of experimental EFISH values is complicated by several issues; among the most important are the use of different conventions to define nonlinear properties and the calibration factors. As for conventions, we follow ref 80, where it has been shown that the EFISH values of pNA in DI reported by Teng and Garito,[81] Stähelin et al.,[82] and Wortmann et al.[8,83] have to be multiplied by a factor of 4 to convert them into the Taylor convention applied here. Note that this is not in accord with the work of Willetts et al.,[84] according to which the correct factor would be 6. It has been shown in ref 80 that the reason for the discrepancy is the fact that Willetts et al. only considered the effects of different conventions for the hyperpolarizabilities in the expression for the molecular dipole moment but did not take into account the existence of different conventions for the *susceptibilities* in the expression for the macroscopic polarization $\underline{P}$, as were, in effect, applied in the cited references.

For HRS, we report the relative values $\langle\beta_{ZZZ}\rangle/\langle\beta_{ZZZ}\rangle_{DI}$ as they have been reported in refs 85 and 86. We also compare the absolute value β_{xxx} of pNA in DI at $\lambda = 1064$ nm with that obtained by Kaatz and Shelton by calibrating with the absolute HRS signal of CCl_4.[87] In the original report, good agreement with previous EFISH results was claimed, assuming that the latter should be multiplied by 2 to convert to the Taylor expansion convention. However, in the following, the calibration factor of the HRS signal of liquid CCl_4 was substantially revised,[12,88] and with the most current calibration factor, the previous results obtained in ref 87 should be multiplied by a factor of 1.88,[80,89] bringing the HRS result in very good agreement with the EFISH values, when the correct factor of 4 is applied.

Additionally, the currently accepted value for the SHG signal of quartz ($\chi_{xxx}(-2\omega;\omega,\omega) = 0.6$ pm/V) was adopted and literature values multiplied with corresponding factors, where appropriate.

Finally, we mention that the solubility of pNA in CH is too small to allow a reliable determination of nonlinear properties. Huyskens et al.[85] performed HRS measurements of pNA in mixtures of *n*% 1-nitropropane in CH, with $n = 10-100\%$. To compare with our computed pNA/CH results, we fitted their results to a polynom of degree three, which was then extrapolated to $n = 0\%$.

Overall, the computed results compare surprisingly well with the experimental values, considering the approximations made in the model. The relative HRS values deviate up to 25% from experiment, while the naturally more difficult to predict absolute EFISH values show deviations up to 33% for pNA/THF. Good agreement is obtained for EFISH of pNA/DI, with a range of predicted values only slightly larger than the spread in the experimental values. The relative HRS signal of pNA/CH is also predicted quite well. The larger deviations for pNA/THF are probably due to the underestimation of the dielectric properties caused by the force field applied in the MD step. It should be mentioned again that the properties of the *optimized* geometry were used in the computation. Generally, we would expect smaller predicted EFISH values if intramolecular flexibilities are taken into account, as found for the gas-phase properties of pNA in ref 11. This would probably affect the properties of the OSCRF-optimized geometry more strongly than those of the IEFPCM-optimized geometry, thus reducing the gap between the predictions for the two geometries.

Jensen and van Duijnen[90] have recently reported a QM/MM study of the first hyperpolarizability of pNA in 1,4-dioxane. In their approach,[91] which is similar to ours, the linear and nonlinear response of a solute molecule is computed quantum mechanically by DFT directly during the simulation. The electrostatic solvent effects are modeled by polarizable point charges, and the molecular response is analyzed by an extended Lorentz local field approach, combined with a statistical average.

TABLE 8: Comparison of Computed and Experimental Microscopic EFISH Signal $\langle\gamma(2\omega)\rangle_E/(10^{-60}$ C^4 m^4 J^{-3}) and Relative (for CH and THF) or Absolute HRS (for DI) Signal in VV Geometry $\langle\beta_{ZZZ}(2\omega)\rangle_{rel/abs}$ of pNA in CH, DI, and THF Solutions

solvent	geom.	ω/au	$\langle\gamma\rangle_E$[a]	exp.	$\langle\beta_{ZZZ}\rangle_{rel/abs}$	exp.
CH	IEFPCM	0.0428	112.7		0.71[b], 0.76[c]	0.85[d],0.76[e]
DI	IEFPCM	0.0239	104.4	86.1[f]		
DI	OSCRF		121.4			
DI	IEFPCM	0.0428	148.4	152.2[f], 165.2[g]	1610	1755[i]
DI	OSCRF		175.4	150.0[h]	1747	
THF	IEFPCM	0.0428	147.9		0.93[b], 1.0[c]	1.12[d]
THF	OSCRF		173.4	219.5[g]	0.99[b], 1.06[c]	1.17 ± 0.07[j]

[a] 10^{-60} C^4 m^4 J^{-3} = 1.6036 × 10^5 au. [b] With OSCRF-optimized geom. of pNA in DI. [c] With IEFPCM-optimized geom. of pNA in DI. [d] 10% 1-nitropropane in cyclohexane; see ref 85. [e] Extrapolated from data in ref 85; see text. [f] Reference 81, assuming μ=2.44 au (refs 8 and 63). [g] Reference 82. [h] Reference 8. [i] Obtained from 2470 × 1.88 × $\sqrt{1/7}$; see refs 87, 88, 80, and 79. [j] Reference 86.

Both the effects of the surrounding molecules as well as those caused by the macroscopic field due to an external applied field can be computed. This approach is in principle more accurate than the one used here, as it takes proper account of (hyper)-polarizability fluctuations due to local field fluctuations and considers explicitly the macroscopic field. On the other hand, it is computationally much more expensive and does not allow large systems and/or long simulation times. An additional problem related specifically to pNA is the rather strongly overestimated frequency dispersion of pNA with DFT using LDA or GGA functionals,[90,92] which prevented a direct comparison of absolute values for $\beta_{||}(2\omega; \omega, \omega)$ with experiment. Thus, only the ratio of $\beta_{||}$ of the solvated pNA molecule and that of the molecule in the gas phase was computed at ω = 0.04283 au and found to be 1.30. This is in good agreement with the results of the HRS values of Kaatz et al.,[87,12] but only with the calibration factor for CCl_4 employed in ref 87, which has been later revised to be 1.88 times larger.[12,88,80] It was assumed that pNA has the same geometry of C_{2v} symmetry in both phases. This value is considerably smaller than the one found here for pNA in the comparable OSCRF geometry, which is about 1.65 (see Table 4 in ref 11 and Table 7). Inspection of the values given in ref 90 shows that this discrepancy is caused by the macroscopic field due to the externally applied field: without this field, the enhancement of $\beta_{||}$ due to the permanent local field is about 2.2, which is even larger than our value, probably at least in part due to overestimation of the dispersion at the DFT level. Inclusion of the macroscopic field in the computation reduces this value again by a factor of 1.7. Such a *decreasing* effect of the macroscopic field on polarizabilities is not predicted at all by continuum local field theories[93] and has been found previously with similar methods in other liquids,[91,93] although it seems particularly large in the case of β of pNA in 1,4-DI. It seems unlikely that this is a confinement effect as observed in ionic crystals,[94] considering the large enhancing effect of the permanent local field alone. Orientational effects are also excluded as explanation as only the frequency-dependent β is predicted and the macroscopic field should thus be of optical frequency.

In our two-step approach, the macroscopic field would only be included implicitly if the susceptibilities were computed. As mentioned above, this is not viable in the case of EFISH on pNA in 1,4-DI due to poor statistics in the MD computation step with an additionally applied static electric field and furthermore also because the nonpolarizable potential used would probably lead to a poor description of the response of pNA to the static field. Thus, to test if in our approach a similar macroscopic field effect occurs, we can apply an additional macroscopic field in our second step, the computation of the permanent local field, and compare the effect with Onsager model predictions. We used macroscopic fields $E_Z^{mac} = 0$ (no field) and $E_Z^{mac} = \pm 0.003$ au along the box direction Z, considered that for conducting boundary conditions and spherical summation the macroscopic field equals the externally applied field,[95,96] applied finite field techniques as in ref 13, and analyzed the local field $\underline{F}_k^{ind}$ induced in molecule k by the macroscopic field according to

$$F_{ki}^{ind} = f_{kii} E_{ki}^{mac} \tag{25}$$

where $i = x, y, z$ denotes the molecular axes. Linear regression of the results obtained over the trajectories gave the average local field factors f_{ii} for pNA shown in Table 9.

TABLE 9: Local Field Factors for pNA Obtained from DLFT Using Externally Applied Fields and from the Onsager (Ons) Model

solvent/geom.		f_{xx}	f_{yy}	f_{zz}
CH/IEFPCM	DLFT	1.276	1.363	1.519
CH	Ons	1.296	1.344	1.494
DI/OSCRF	DLFT	1.315	1.439	1.578
DI	Ons	1.328	1.383	1.557
THF/OSCRF	DLFT	1.281	1.359	1.462
THF	Ons	1.287	1.333	1.476

The corresponding local field factors in the ellipsoidal Onsager continuum model are obtained from[75]

$$f_{ii}^{Ons} = f_{ii}^{C\omega}(1 - f_{ii}^{R\omega}\alpha_{ii}(\omega))^{-1} \tag{26}$$

where $f_{ii}^{R\omega}$ are defined analogously as in eq 23 and the cavity factors $f_{ii}^{C\omega}$ are given by

$$f_{ii}^{C\omega} = \frac{n^2(\omega)}{n^2(\omega) - \kappa_i(n^2(\omega - 1))} \tag{27}$$

As the macroscopic field is applied to the rigid snapshots, that is, cannot induce molecular reorientation, the refractive indices instead of the relative permittivity are used in these equations. Using the same parameters for pNA as in the permanent local field calculation above, one obtains the values given in Table 9. Comparison of the DLFT and Onsager local field factors shows that they agree extremely well: in most cases, the deviations are smaller than 2%, only for f_{yy} in DI do we find a deviation of 4%. Thus, our model does not confirm the findings of Jensen and van Duijnen concerning the shortcomings of continuum models in modeling the effect of macroscopic fields. Especially noteworthy is that the *components* agree very well, not just the average values. This is probably a reflection of the approximately ellipsoidal shape of the pNA molecule.

Cascading Effects on the THG Signal of pNA in THF. Meredith and Buchalter[47] measured the concentration dependence of the third harmonic generation signal of pNA in several

polar solvents and found a strong concentration dependence of γ, when the signals were interpreted as being caused only by the so-called direct term (cf. eq 13). This behavior was attributed to the cascading term, arguing that this term is concentration dependent, while the direct term is not, implying that α and γ do not depend on concentration. Thus, it was found that the cascading term makes a substantial contribution to the THG signal. Another possible explanation would involve the permanent local field, which could be different in the different solutions and changes α and γ, thus invalidating to a certain degree the assumption that the direct term is independent of pNA concentration. We computed the direct and cascading terms contributing to $\chi^{(3)}_{ZZZZ}(-3\omega; \omega, \omega, \omega)$ of THG on pNA in THF according to eq 13, using the molecular properties computed for the EFISH process as a reasonable approximation. The result, computed as an average over the three diagonal components, is $\chi^{(3)}_{ZZZZ}{}^{,\text{direct}} = 271.6$ (pm/V)^2 and $\chi^{(3),\text{casc}}_{ZZZZ} = 1.4$ (pm/V)^2, showing that the cascading contribution is practically negligible here. Although THF is much less polar than the solvents employed in ref 47 and the mole fraction of pNA THF (0.0033) is on the lower side of those employed by Meredith and Buchalter, our result indicates that the cascading contribution seems to be of little importance for solutions of pNA.

4. Summary

Solutions of pNA in solvents of different dominant multipolar character as well as the pure solvents itself were simulated in this work, and the local field effects on linear and nonlinear optical properties were investigated in quadrupolar and hexadecapolar approximation in a discrete and polarizable description of the molecular electrostatic interactions in the liquid, using accurately computed multipole moments and molecular polarizabilities up to quadrupole−quadrupole computed at the ab initio level. The model employs a two-step approach, where in the first step, liquid configurations are obtained by nonpolarizable classical molecular dynamics simulations, which are analyzed in the second step using a fully polarized description.

For the pure solvents, a very good agreement between simulated and experimental linear optical properties was obtained, as well as a good to reasonable agreement in the much more difficult to simulate high-order process of third harmonic generation (THG). The predicted static dielectric constant in THF was found to be too low, a failure which may be attributed to the employed OPLS-AA potential in the simulation step.

By the use of a simple model to describe the distribution of electric properties over pNA, the average local field and field gradient is obtained with a good convergence with respect to the order of multipole expansion. In all three solvents, the permanent local field is essentially converged at the quadrupolar approximation, which generally changes results obtained at the dipole approximation considerably. This holds especially for 1,4-dioxane solvent, where the permanent quadrupoles of the solvent contribute about 50% to the permanent local field. At the dipolar level, 1,4-dioxane yields similar field values as the nonpolar solvent cyclohexane; including quadrupole as well as quadrupole polarizabilities, the fields are similar to those obtained in the polar solvent THF.

When the molecular properties with the obtained permanent local field and gradient were computed, it was found that the gradient contribution is negligible, and with only the local field taken into account, a surprisingly good agreement with experimental EFISH and HRS values in the solvents investigated is obtained, if comparisons between experimental and theoretical values are done in accordance with the recently revised conversion factors.[80] The largest deviations were found again in THF solvent and may be explained by the failure of the employed potential in the molecular dynamics simulation to model the dielectric constant of this solvent, thus leading to a too low permanent local field on pNA. It could also be shown that the ellipsoidal Onsager model with an "effective" permittivity $\epsilon_r = 6$ for 1,4-dioxane is able to describe local field factors as well as the permanent local field on the solute in good agreement with discrete local field theory. The good performance of the continuum Onsager model may at least in part be due to the approximately ellipsoidal shape of the pNA molecule. The very good agreement of the Onsager local field factors with those obtained from a statistical analysis of the discrete model system subjected to additional macroscopic fields is in contrast to results reported recently by Jensen and van Duijnen,[90] who employed a similar method, called the discrete reaction field model, for a solution of pNA in 1,4-dioxane, and found that the additional macroscopic field leads to a strong *decrease* of the solute hyperpolarizability, which is not accounted for by the Lorentz−Onsager local field factors. The discrepancy between their results and ours warrants further investigation.

Together with the results in the first part[11] of this series, this work shows that the linear and nonlinear optical properties of pNA in the gas phase as well as in solution can be predicted in reasonably good agreement with experiment using our model. In agreement with previous studies on linear effects, we found that the "dioxane anomaly" affects also the nonlinear optical properties as expected. It was found that the unusual solvent effect in 1,4-dioxane solution is primarily due to large permanent

TABLE 10: OPLS-AA Potential Parameters of CH, DI, and THF Used in the Molecular Dynamics

partial charges q (1 e = 1.6022 × 10^{-19} C), $U_{\text{LJ},ij} = 4\epsilon_{ij}[(\sigma_{ij}/r_{ij})^{12} - (\sigma_{ij}/r_{ij})^6]$

atom type	bonding	q (e)	σ_{ii} (Å) [a]	ϵ_{ii} (kcal/mol)[a]
CT	R−CH_2−OR	0.140	3.500	0.066
	R_2CH_2	−0.120		
HC	RHC−HOR	0.030	2.500	0.030
	H−C(Alkyl)	0.060		
OS	R−O−R′	−0.400	2.900	0.140

$U_b = k_l(r - r_0)^2$

bond	r_0 (nm)	k_l (kcal mol^{-1} Å^{-2})
CT−CT	1.529	268.0
CT−HC	1.090	340.0
CT−OS	1.410	320.0

$U_a = k_\theta(\theta - \theta_0)^2$

angle	θ_0 (deg)	k_θ (kcal mol^{-1} rad^{-2})
CT−C−CT	112.7	58.35
CT−CT−HC	110.7	37.50
CT−CT−OS	109.5	50.00
CT−OS−CT	109.5	60.00
HC−CT−OS	109.5	35.00
HC−CT−HC	107.8	33.00

$U_t \sum_{n=1}^{3} V_n/2[1 + (-1)^{n+1}\cos(n\phi)]$; all V_n in kcal mol^{-1}

proper torsion	V_1	V_2	V_3
CT−CT−CT−CT	1.300	−0.050	0.200
CT−CT−CT−HC	0.000	0.000	0.300
CT−CT−CT−OS	1.711	−0.500	0.663
CT−OS−CT−CT	0.650	−0.250	0.670
HC−CT−CT−HC	0.000	0.000	0.300
HC−CT−CT−OS	0.000	0.000	0.468
HC−CT−OS−CT	0.000	0.000	0.760
OS−CT−CT−OS	0.000	1.150	0.000

[a] Cross terms are computed by $\epsilon_{ij} = (\epsilon_{ii}\epsilon_{jj})^{1/2}$ and $\sigma_{ij} = (\sigma_{ii}\sigma_{jj})^{1/2}$.

TABLE 11: Potential Parameters for pNA Used in the Molecular Dynamics

partial charges q (1 e = 1.6022×10^{-19} C),
$U_{LJ,ij} = 4\epsilon_{ij}[(\sigma_{ij}/r_{ij})^{12} - (\sigma_{ij}/r_{ij})^{6}]$

atom type	bonding	q (e)	σ_{ii} (Å)[a]	ϵ_{ii} (kcal/mol)[a]
	C−CNO_2	−0.1463		
CA	C−CNH_2	−0.3454		
	C−NH_2	0.5334	3.550	0.070
	C−NO_2	0.0266		
HA	H−C(Aryl)	0.1898	2.420	0.030
HN	H−N	0.3986	0.000	0.000
NO	Ar−NO_2	0.7561	3.250	0.120
NT	Ar−NH_2	−0.9479	3.296	0.120
ON	NO_2	−0.4706	2.960	0.170

$U_b = k_l(r - r_0)^2$

bond	r_0 (nm)	k_l (kcal mol^{-1} Å^{-2})
CA−CA	1.400	469.0
CA−HA	1.080	367.0
CA−NT	1.340	481.0
CA−NO	1.460	400.0
NT−HN	1.010	434.0
NO−ON	1.225	500.0

$U_a = k_\theta(\theta - \theta_0)^2$

angle	θ_0 (deg)	k_θ (kcal mol^{-1} rad^{-2})
CA−CA−CA	120.0	63.00
CA−CA−HA	120.0	35.00
CA−CA−NT	120.1	70.00
CA−CA−NO	120.0	85.00
CA−NT−HN	111.0	35.00
HN−NT−HN	106.4	43.60
CA−NO−ON	117.5	80.00
ON−NO−ON	125.0	80.00

$U_t = \sum_{n=1}^{3} V_n/2[1 + (-1)^{n+1}\cos(n\phi)]$; all V_n in kcal mol^{-1}

proper torsion	V_1	V_2	V_3
CA−CA−CA−X	0.000	7.250	0.000
HA−CA−CA−X	0.000	7.250	0.000
CA−CA−NT−HN	0.000	2.500	0.000
CA−CA−NO−ON	0.000	6.835	0.000
improper torsion			
CA−CA−CA−X	0.000	2.200	0.000
HA−CA−CA−X	0.000	2.200	0.000
CA−CA−X−CA	0.000	2.200	0.000
ON−ON−NO−CA	0.000	21.000	0.000
HN−CA−NT−HN	58.464	−27.667	5.250

[a] Cross terms are computed by $\epsilon_{ij} = (\epsilon_{ii}\epsilon_{jj})^{1/2}$ and $\sigma_{ij} = (\sigma_{ii}\sigma_{jj})^{1/2}$.

quadrupole moments of the solvent but also induced effects are not negligible. Nevertheless, it should be kept in mind that error cancellations may lead to artificially good agreement with experiment and improvements of our model are possible and should be pursued to minimize the sources of error. For example, the comparison between predicted and experimental microscopic EFISH values still relies on the accuracy of the Onsager−Lorentz factor approach used to extract the experimental values. A more stringent test would be the prediction of the EFISH susceptibilities, which in the DFLT approach would require the inclusion of the reorienting static field in the molecular simulation step. To achieve a reliable prediction, it would then be necessary to use more sophisticated force fields, which should be polarizable, and should also be able to describe intramolecular charge-transfer effects in conjunction with intramolecular structure changes accurately. Additionally, it would then be necessary to describe the effects of intramolecular geometry changes on multipole moments and the (hyper)polarizabilities in the induction part of the calculation, for example, in the spirit of the dipole or monopole−dipole interaction models developed by Jensen et al.[97] or Applequist.[98]

Note Added in Proof: While this paper was in the proof stage, a molecular dynamics simulation probing the 1,4-dioxane anomaly by way of the solvatochromism of coumarin 153 was published by Cinacchi, Ingrosso, and Tani (*J. Phys. Chem. B.* **2006**, *110*, 13633). The authors come to similar conclusions regarding the origin of the dioxane anomaly as we did. Employing a slightly different potential for 1,4-dioxane, they report even better agreement between simulated and neutron diffraction measurements for pure 1,4-dioxane liquid.

Acknowledgment. We gratefully acknowledge financial support from the European Commission in the form of a Marie Curie Development Host Fellowship (HPMD-CT-2001-00091) and from the HPC Europa Transnational Access Program (Contract No. RII3-CT-2003-506079). H.R. acknowledges support from the European Center for Parallelism of Barcelona (CEPBA), where a part of the reported computations were performed. H.R. further thanks Prof. Takamuku for providing the experimental values of the radial distribution functions of 1,4-dioxane and THF.

Appendix

The OPLS-AA potential parameters for CH, DI, and THF used are given in Table 10, those for pNA are given in Table 11. The parameters were taken from refs 21 and 22 except for the partial charges, the improper torsion HN−CA−NT−HN and the proper torsion CA−CA−NO−ON of pNA. The dipole moment of pNA computed with the partial charges taken from the cited references was nearly a factor of 2 too small compared with the ab initio result, therefore the charges were recomputed employing the charge fit procedure available in Gaussian 98,[99] which fits atomic charges to the electrostatic potential on the van der Waals surface. To be consistent with the other OPLS-AA parameters,[100] they were determined at the RHF/6-31G*//RHF/6-31G* level, where the molecule adopts C_s symmetry.

For the determination of the nitro torsional parameters, we used the results of ref 11, where we reported the energies of partially optimized structures with the nitro dihedral angle scanned. For the amino proper torsion and improper torsions, we performed new 6-31G*/SCF computations. For the determination of the Fourier amplitudes, the procedure advocated by Jorgensen et al.[23] was employed. The charge parameters were not adjusted to obtain better fits.

References and Notes

(1) Reynolds, L.; Gardecki, J. A.; Frankland, S. J. V.; Horng, M. L.; Maroncelli, M. *J. Phys. Chem.* **1996**, *100*, 10337.
(2) Khajehpour, M.; Kauffman, J. F. *J. Phys. Chem. A* **2000**, *104*, 9512.
(3) Bischof, H.; Baumann, W.; Detzer, N.; Rotkiewicz, K. *Chem. Phys. Lett.* **1985**, *116*, 180.
(4) Baumann, W.; Nagy, Z.; Maiti, A. K.; Reis, H.; Vianna Rodrigues, S.; Detzer, N. In *Dynamics and Mechanism of Photoinduced Transfer and Related Phenomena*; Mataga, N., Okada, T., Masuhara, H., Eds.; Elsevier New York, 1992; p 211.
(5) Geerlings, J. D.; Varma, C. A. G. O.; van Hemert, M. C. *J. Phys. Chem. B* **2000**, *104*, 56.
(6) Khajehpour, M.; Kauffman, J. F. *J. Phys. Chem. A* **2001** *105*, 10316.
(7) Baumann, W. In *Physical Methods of Chemistry, Determination of Chemical Composition and Molecular Structure 2E*; Rossiter, B. W., Hamilton, J. F., Eds.; Wiley: New York, 989; Vol. 3B, p 45.
(8) Wortmann, R.; Krämer, P.; Glania, C.; Lebus, S.; Detzer, N. *Chem. Phys.* **1993**, *99*, 173.
(9) Liptay, W. *Z. Naturforsch. A: Phys. Sci.* **1965**, *20*, 1441.
(10) Ledger, M. B.; Suppan P. *Spectrochim. Acta, Part A* **1967**, *23*, 3007.

(11) Reis, H.; Grzybowski, A.; Papadopoulos, M. G. *J. Phys. Chem. A* **2005** *109*, 10106.
(12) Kaatz, P.; Donley, E. A.; Shelton, D. P. *J. Chem. Phys.* **1998**, *108*, 849.
(13) Janssen, R. H. C.; Bomont, J.-M.; Theodorou, D. N.; Raptis, S.; Papadopoulos, M. G. *J. Chem. Phys.* **1999**, *110*, 6463.
(14) Janssen, R. H. C.; Theodorou, D. N.; Raptis, S.; Papadopoulos, M. G. *J. Chem. Phys.* **1999**, *111*, 9711.
(15) Reis, H.; Papadopoulos, M. G.; Theodorou, D. N. *J. Chem. Phys.* **2001**, *114*, 876.
(16) Batista, E. R.; Xantheas, S. S.; Jónsson, H. *J. Chem. Phys.* **1998** *109*, 4546.
(17) Batista, E. R.; Xantheas, S. S.; Jónsson, H. *J. Chem. Phys.* **1999** *111*, 6011.
(18) Batista, E. R.; Xantheas, S. S.; Jónsson, H. *J. Chem. Phys.* **2000** *112*, 3285.
(19) Smith, W.; Leslie, M.; Forrester, T. R. DL_POLY 2.14, CCLRC, Daresbury Laboratory: Daresbury, Warrington, U.K., 2003.
(20) Nosé, S. *Mol. Phys.* **1984**, *52*, 255. Hoover, W. G. *Phys. Rev. A* **1985**, *31*, 1695. Melchionna, S.; Ciocotti, G.; Holian, B. L. *Mol. Phys.* **1993**, *78*, 533.
(21) Jorgensen, W. L.; Laird, E. R.; Nguyen, T. B.; Tirado-Rives, J. *J. Comput. Chem.* **1993**, *14*, 206.
(22) Wang, J.; Cieplak, P.; Kollman, P. A. *J. Comput. Chem.* **2000**, *21*, 1049.
(23) Jorgensen, W. L.; Maxwell, D. S.; Tirado-Rives, J. *J. Am. Chem. Soc.* **1996**, *118*, 11225.
(24) Jorgensen, W. L. OPLS All-Atom Force Field, parameter files oplsaa.par and oplsaa.sb, distributed with the BOSS program, Yale University, New Haven, CT, March 2004.
(25) Applequist. *Chem. Phys.* **1984**, *85*, 279; errata: *Chem. Phys.* **1995**, *190*, 153.
(26) Dykstra, C.; Liu, S.-L.; Malik, D. J. *Adv. Chem. Phys.* **1989**, *75*, 37.
(27) Logan, D. E. *Mol. Phys.* **1982**, *46*, 271.
(28) Gunning, M. J.; Raab, R. E. *Mol. Phys.* **1997**, *91*, 589.
(29) Buckingham, A. D. *Adv. Chem. Phys.* **1967**, *12*, 107.
(30) Cummins, P. G.; Dunmur, D. A.; Munn, R. W.; Newham, R. J. *Acta Crystallogr., Sect. A: Found. Crystallogr.* **1976**, *32*, 847.
(31) Jansen, G.; Hättig, C.; Hess, B. A.; Ángyán, J. *Mol. Phys.* **1996**, *88*, 69.
(32) Claverie, P. In *Intermolecular Interactions: From Diatomic to Biopolymers*; Pullman, B., Ed.; Wiley: Chichester, U.K., 1978; pp 69−306.
(33) LeSueur, C. R.; Stone, A. J. *Mol. Phys.* **1993**, *78*, 1267.
(34) Stone, A. J. *The Theory of Intermolecular Forces*, Clarendon: Oxford, U.K., 1996.
(35) Ángyán, J. G.; Jansen, G.; Loos, M.; Hättig C.; Hess, B. A. *Chem. Phys. Lett.* **1994**, *219*, 267.
(36) Reis, H.; Papadopoulos, M. G.; Hättig, C.; Ángyán, J. G.; Munn, R. W. *J. Chem. Phys.* **2000**, *112*, 6161.
(37) in het Panhuis, M.; Munn, R. W.; Popelier, P. L. A. *J. Chem. Phys.* **2004**, *120*, 11479.
(38) Luty, T. *Chem. Phys. Lett.* **1976**, *44*, 335.
(39) Bounds, P. J.; Munn, R. W. *Chem. Phys.* **1981**, *59*, 47.
(40) Reis, H.; Papadopoulos, M. G.; Calaminici, P.; Jug, K.; Köster, A. M. *Chem. Phys.* **2000**, *261*, 359.
(41) Reis, H.; Makowska-Janusik, M.; Papadopoulos, M. G. *J. Phys. Chem. B* **2004**, *108*, 8931.
(42) Caillol, J. M.; Levesque, D.; Weis, J. J.; Kusalik, R. G.; Patey, G. N. *Mol. Phys.* **1985**, *55*, 65.
(43) Hurst M.; Munn, R. W. *J. Mol. Electron.* **1983**, *2*, 35, 43.
(44) Malagoli, M.; Munn, R. W. *J. Chem. Phys.* **1997**, *107*, 7926.
(45) Reis, H.; Papadopoulos, M. G.; Munn, R. W. *J. Chem. Phys.* **1998**, *109*, 6828.
(46) Reis, H.; Papadopoulos, M. G. In *Nonlinear Optical Responses of Molecules, Solids and Liquids: Methods and Applications*; Papadopoulos, M. G., Ed.; Trivandrum 2003, Research Signpost.
(47) Meredith, G. R.; Buchalter, B. *J. Chem. Phys.* **1983**, *78*, 1938.
(48) Butcher, P. N.; Cotter, D. *The Elements of Nonlinear Optics*; Cambridge University Press: Cambridge, U.K., 1990.
(49) Shelton, D. P.; Rice, J. E. *Chem. Rev.* **1994**, *94*, 3.
(50) Kneller, G. K. *Mol. Simul.* **1991**, *7*, 113.
(51) Cancés, E.; Mennucci, B.; Tomasi, J., *J. Chem. Phys.* **1997**, *107*, 3032.
(52) Maier, V.; Svoboda, V. *Enthalpies of Vaporization of Organic Liquids: A Critical Review and Data Compilation*; Blackwell: Oxford, U.K., 1985.
(53) Wortmann, R. *Habilitationsschrift*, Mainz, Germany, 1993.
(54) Chapman, D. M.; Hester, R. E. *J. Chem. Phys. A* **1997**, *101*, 3382.
(55) Takamuku, T.; Yamaguchi, A.; Tabata, M.; Nishi, N.; Yoshida, K.; Wakita, H.; Yamagushi, T. *J. Mol. Liq.* **1999**, *83*, 163.
(56) Takamuku, T.; Nakamizo, A.; Tabata, M.; Yoshida, K.; Yamagushi, T.; Otomo, T. *J. Mol. Liq.* **2003**, *103*−*104*, 143.
(57) Farman, H.; Dore, J. C.; Bellisent-Funel, M.-C.; Montagne, D. G. *Mol. Phys.* **1987**, *61*, 583.
(58) Bertagnolli, H.; Chieux, P.; Zeidler, M. D. *Mol. Phys.* **1976**, *32*, 759.
(59) Warren, B. E.; Krutter, H.; Morningstar, O. *J. Am. Ceram. Soc.* **1936**, *19*, 202.
(60) *International Tables for Crystallography*; Hahn, T, Ed.; Reidel: Boston, 1983; Vol. 4.
(61) Kajzar, F.; Messier, J. *Phys. Rev. A* **1985**, *32*, 2352.
(62) Burland, D. M.; Walsh, C. A.; Kajzar, F.; Sentein, C. *J. Opt. Soc. Am. B* **1991**, *8*, 2269.
(63) Cheng, L.-T.; Tam, W.; Stevenson, S. H.; Meredith, G. R.; Rikken, G.; Marder, S. R. *J. Phys. Chem.* **1991**, *95*, 10631.
(64) Hurwic, J.; Pelliccia-Galand, M.-F. *C. R. Acad. Sci., Ser. IIc: Chim.* **1972**, *275*, 1073. Pelliccia-Galand, M.-F.; Hurwic, J. *C. R. Acad. Sci., Ser. IIc: Chim.* **1973**, *277*, 137. Hurwic, J.; Pelliccia-Galand, M.-F. *C. R. Acad. Sci. Ser. IIc: Chim.* **1975**, *280*, 1.
(65) Saiz, L.; Guàrdia, E.; Padró, J. *J. Chem. Phys.* **2000**, *113*, 2814.
(66) Richardi, J.; Fries, P. H.; Krienke, H. *J. Phys. Chem. B* **1998**, *102*, 5196.
(67) Meredith, G. R.; Buchalter, B.; Hanzlik, C. *J. Chem. Phys.* **1982**, *78*, 1543.
(68) Bosshard, C.; Gubler, U.; Kaatz, P.; Mazerant, W.; Meier, U. *Phys. Rev. A* **2000**, *61*, 10688.
(69) Buchalter, B.; Meredith, G. R. *Appl. Opt.* **1982**, *21*, 3221.
(70) Mito, A.; Hagimoto, K.; Takahashi, C. *Nonlinear Opt.* **1995**, *13*, 3.
(71) Huyskens, F.; Morissen, H.; Huyskens, P. *J. Mol. Struct.* **1998**, *441*, 17.
(72) Moylan, C. R.; Miller, R. D.; Twieg, R. J.; Lee, V. Y. *ACS Symp. Ser.* **1994**, *601*, 66.
(73) Ahlström, P.; Wallqvist, A.; Engström, S.; Jönsson, B. *Mol. Phys.* **1989**, *68*, 563.
(74) Böttcher, C. J. F. *Theory of Electric Polarization*, 2nd ed.; Elsevier: Amsterdam, The Netherlands, 1973.
(75) Wortmann, R.; Bishop, D. M. *J. Chem. Phys.* **1998**, *108*, 1001.
(76) Cammi, R.; Mennucci, B.; Tomasi, J. *J. Phys. Chem.* **2000**, *104*, 4690.
(77) Sadlej, A. J. *Collect. Czech. Chem. Commun.* **1988**, *53*, 1995.
(78) Munn R. W.; Luo, Y.; Macak, P.; Ågren, H. *J. Chem. Phys.* **2001**, *114*, 3105.
(79) Bersohn, R.; Pao, Y.-H.; Frisch, H. L. *J. Chem. Phys.* **1966**, *45*, 3184.
(80) Reis, H. *J. Chem. Phys.* **2006**, *125*, 014506.
(81) Teng, C. C.; Garito, A. F. *Phys. Rev. B* **1983**, *28*, 6766.
(82) Stähelin, M.; Burland, D. M.; Rice, J. E. *Chem. Phys. Lett.* **1992**, *191*, 245.
(83) The conventions applied in ref 8 can be derived from Wortmann, R. *Habilitationsschrift*, Mainz, Germany, 1993.
(84) Willetts, A.; Rice, J. E.; Burland, D. M.; Shelton, D. *J. Chem. Phys.* **1992**, *97*, 7590.
(85) Huyskens, F. L.; Huyskens, P. L.; Persoons, A. *J. Chem. Phys.* **1998**, *108*, 8161.
(86) Kodaira, T.; Watanabe, A.; Ito, O.; Matsuda, M.; Clays, K.; Persoons, A. *J. Chem. Soc., Faraday Trans.* **1997**, *93*, 3039.
(87) Kaatz, P.; Shelton, D. P. *J. Chem. Phys.* **1996**, *105*, 3918.
(88) Pyatt, R. D.; Shelton, D. P. *J. Chem. Phys.* **2001**, *114*, 9938.
(89) Shelton, R. D. Private Communication.
(90) Jensen, L.; van Duijnen, P. Th. *J. Chem. Phys.* **2005**, *123*, 074307.
(91) Jensen, L.; Swart, M.; van Duijnen, P. Th. *J. Chem. Phys.* **2005**, *122*, 034103.
(92) van Gisbergen, A. J. A.; Snijders, J. G.; Baerends, E. J. *J. Chem. Phys.* **1998**, *109*, 10644; erratum: *J. Chem. Phys.* **1999**, *111*, 6652.
(93) van Duijnen, P. Th.; de Vries, A. H.; Swart, M.; Grozema, F. *J. Chem. Phys.* **2002**, *117*, 8442.
(94) Jemmer, P.; Fowler, P. W.; Wilson, M.; Madden, P. A. *J. Phys. Chem. A* **1998**, *102*, 8377.
(95) Neumann, M. *Mol. Phys.* **1983**, *50*, 841.
(96) de Leeuw, S. W.; Perram, J. W.; Smith, E. R. *Annu. Rev. Phys. Chem.* **1986**, *37*, 245.
(97) Jensen, L.; Sylvester-Hvid, K. O.; Mikkelsen, K. V.; Åstrand, P.-O. *J. Phys. Chem. A* **2003**, *107*, 2270.
(98) Applequist, J. *J. Chem. Phys.* **1985**, *83*, 809.
(99) Frisch, M. J.; Trucks, G. W.; Schlegel, H. B.; Scuseria, G. E.; Robb, M. A.; Cheeseman, J. R.; Zakrzewski, V. G.; Montgomery, J. A.; Stratmann, R. E.; Burant, J. C.; Dapprich, S.; Millam, J. M.; Daniels, A. D.; Kudin, K. N.; Strain, M. C.; Farkas, O.; Tomasi, J.; Barone, V.; Cossi, M.; Cammi, R.; Mennucci, B.; Pomelli, C.; Adamo, C.; Clifford, S.; Ochterski, J.; Petersson, G. A.; Ayala, P. Y.; Cui, Q.; Morokuma, K.; Malick, D. K.; Rabuck, A. D.; Raghavachari, K.; Foresman, J. B.; Cioslowski, J.; Ortiz, J.

V.; Stefanov, B. B.; Liu, G.; Liashenko, A.; Piskorz, P.; Komaromi, I.; Gomperts, R.; Martin, R. L.; Fox, D. J.; Keith, T.; Al-Laham, M. A.; Peng, C. Y.; Nanayakkara, A.; Gonzalez, C.; Challacombe, M.; Gill, P. M. W.; Johnson, B. G.; Chen, W.; Wong, M. W.; Andres, J. L.; Head-Gordon, M.; Replogle E. S.; Pople, J. A. *Gaussian 98*, revision A.9; Gaussian, Inc.: Pittsburgh, PA, 1998.

(100) Price, M. L. P.; Ostrovsky, D.; Jorgensen, W. L. *J. Comput. Chem.* **2001**, *22*, 1340.

(101) Brocos, P.; Calvo, E.; Amigo, A.; Bravo, R.; Pintos, M.; Roux, A. H.; Roux-Desgranges, G. *J. Chem. Eng. Data* **1998**, *43*, 112.

(102) Viscotek Corp., Houston, www.viscotek.com/viscosities.php4, extrapolated from Data at 273.15 K given in R. Gant, LC/GC **1992**, *10*, 550, using an expansion coefficient of 0.12% per degree.

(103) *Landolt-Börnstein*, II/5a; Hellwege, K.-H., Hellwege, A. M., Eds.; Springer: Berlin, 1969; p 590.

(104) *Landolt-Börnstein*, II/5a; Hellwege, K.-H., Hellwege, A. M., Eds.; Springer: Berlin, 1969; p 592.

(105) Gisser, D. J.; Johnsen, B. S.; Ediger, M. D.; von Meerwall, E. D. *Macromolecules* **1993**, *26*, 512.

(106) Goldammer, E. V.; Zeidler, M. D. *Ber. Bunsen-Ges. Phys. Chem.* **1969**, *73*, 4.

(107) Hartshorn, L.; Parry, J. V. L.; Essen, L. *Proc. Phys. Soc. B* **1955**, *68*, 422.

(108) *Handbook of Chemistry and Physics*, 62nd ed.; CRC: Boca Raton, FL, 1981.

(109) Stähelin, M.; Moylan, C. R.; Burland, D. M.; Willetts, A.; Rice, J. E.; Shelton, D. P.; Donley, E. A. *J. Chem. Phys.* **1993**, *98*, 5595.